Received: 19 January 2018 | Revised: 14 August 2018 | Accepted: 1 September 2018

DOI: 10.1002/fld.4681

RESEARCH ARTICLE

WILEY

A divergence-free semi-implicit finite volume scheme for ideal, viscous, and resistive magnetohydrodynamics

M. Dumbser[1] | D.S. Balsara[2] | M. Tavelli[1] | F. Fambri[1]

[1]Department of Civil and Environmental Engineering, University of Trento, Trento, Italy

[2]Physics Department, University of Notre Dame du Lac, Notre Dame, Indiana

Correspondence

M. Dumbser, Department of Civil and Environmental Engineering, University of Trento, Via Mesiano, 77, 38123 Trento, Italy.
Email: michael.dumbser@unitn.it

D.S. Balsara, Physics Department, University of Notre Dame du Lac, 225 Nieuwland Science Hall, Notre Dame, IN 46556, Indiana.
Email: dbalsara@nd.edu

M. Tavelli, Department of Civil and Environmental Engineering, University of Trento, Via Mesiano, 77, 38123 Trento, Italy.
Email: m.tavelli@unitn.it

F. Fambri, Department of Civil and Environmental Engineering, University of Trento, Via Mesiano, 77, 38123 Trento, Italy.
Email: francesco.fambri@unitn.it

Funding information

European Research Council (ERC), Grant/Award Number: 278267; European Union's Horizon 2020 Research and Innovation Programme, Grant/Award Number: 671698

Summary

In this paper, we present a novel *pressure-based* semi-implicit finite volume solver for the equations of *compressible* ideal, viscous, and resistive magnetohydrodynamics (MHD). The new method is conservative for mass, momentum, and total energy, and in multiple space dimensions, it is constructed in such a way as to respect the divergence-free condition of the magnetic field exactly, also in the presence of resistive effects. This is possible via the use of multidimensional Riemann solvers on an appropriately staggered grid for the time evolution of the magnetic field and a double curl formulation of the resistive terms. The new semi-implicit method for the MHD equations proposed here discretizes the nonlinear convective terms as well as the time evolution of the magnetic field *explicitly*, whereas all terms related to the pressure in the momentum equation and the total energy equation are discretized *implicitly*, making again use of a properly staggered grid for pressure and velocity. Inserting the discrete momentum equation into the discrete energy equation then yields a *mildly nonlinear* symmetric and positive definite algebraic system for the pressure as the only unknown, which can be efficiently solved with the (nested) Newton method of Casulli et al. The pressure system becomes *linear* when the specific internal energy is a linear function of the pressure. The time step of the scheme is restricted by a CFL condition based only on the fluid velocity and the Alfvén wave speed and is not based on the speed of the magnetosonic waves. Being a semi-implicit pressure-based scheme, our new method is therefore particularly well suited for low Mach number flows and for the incompressible limit of the MHD equations, for which it is well known that explicit *density-based* Godunov-type finite volume solvers become increasingly inefficient and inaccurate because of the more and more stringent CFL condition and the wrong scaling of the numerical viscosity in the incompressible limit. We show a relevant MHD test problem in the low Mach number regime where the new

semi-implicit algorithm is a factor of 50 faster than a traditional explicit finite volume method, which is a very significant gain in terms of computational efficiency. However, our numerical results confirm that our new method performs well also for classical MHD test cases with strong shocks. In this sense, our new scheme is a true *all Mach number* flow solver.

KEYWORDS

all Mach number flow solver, compressible low Mach number flows, divergence-free, finite volume schemes, general equation of state, ideal magnetohydrodynamics, pressure-based method, semi-implicit, viscous and resistive MHD

1 | INTRODUCTION

Since their invention by Harlow and Welch,[1] pressure-based semi-implicit finite difference schemes on staggered grids have become widespread over the last decades for the solution of the incompressible Navier-Stokes equations with and without moving free surface, see, eg, other works,[2-14] for a nonexhaustive overview of some of the most important contributions. An early application of semi-implicit schemes to compressible gas dynamics was the method of Casulli and Greenspan,[15] but their scheme was not conservative and therefore unable to solve problems including shock waves. In the field of numerical methods for high Mach number compressible flows, typically explicit density-based Godunov-type finite volume schemes[16-25] are preferred, since they are by construction conservative and thus allow the correct computation of shock waves. Therefore, the application of semi-implicit methods to compressible flows with shock waves is still quite rare, and some recent developments in this direction have been made only very recently in other works,[26-31] where new *conservative* pressure-based semi-implicit schemes have been proposed that are also suitable for the simulation of flow problems including shock waves. Concerning the numerical simulation of compressible magnetized plasma flows governed by the ideal or viscous and resistive magnetohydrodynamics (MHD) equations, only very little work has been done so far concerning the development of semi-implicit schemes. The existing semi-implicit schemes for MHD either apply only to the incompressible or anelastic case, or they are not based on a conservative formulation, see, eg, other works.[32-36] The declared aim of this paper is therefore to close this gap and to propose a new conservative and pressure-based semi-implicit finite volume method for the solution of the compressible ideal and viscous and resistive MHD (VRMHD) equations that applies both to high Mach number flows with shocks as well as to low Mach number or even incompressible flows. It is well known that explicit density-based solvers become increasingly inefficient and inaccurate in the low Mach number regime and therefore an implicit time discretization is needed. However, discretizing all terms implicitly would lead to a *highly nonlinear* nonsymmetric system with a large number of unknowns (density, velocity, pressure, and magnetic field), for which convergence is very difficult to control. Therefore, the new semi-implicit finite volume (SIFV) method proposed in this paper uses instead an explicit discretization for all nonlinear convective terms and for the time evolution of the magnetic field, whereas an implicit discretization is only employed for the pressure terms. This judicious combination leads in the end to only one *mildly nonlinear* and *symmetric positive definite* system for the fluid pressure as the only unknown. The properties of the pressure system allow the use of the Newton-type techniques of Casulli et al,[37-40] for which convergence has been *rigorously proven*. Due to the implicit pressure terms, the time step of our new scheme is only restricted by the fluid velocity and the Alfvén wave speed, and not by the speeds of the magnetosonic waves. For this reason, the method proposed in this paper is a true *all Mach number* flow solver. We emphasize again that compared to a fully implicit density-based scheme, the chosen semi-implicit pressure-based method has several advantages: (i) in our scheme, the scalar pressure field at the new time level is the only unknown, whereas in fully implicit density-based solvers, the entire state vector of the MHD equations with its eight quantities is unknown; this choice substantially simplifies the solution of the final equation system in our semi-implicit approach compared to a fully implicit one; (ii) the final pressure system of the proposed semi-implicit scheme is only *mildly nonlinear* for general equations of state (EOS), and it is even *linear* for the ideal gas EOS; in contrast, the resulting algebraic system of a fully implicit scheme for the MHD equations is always highly nonlinear; (iii) the pressure system in our scheme is symmetric

and positive definite and the stencil involves only the cell and its direct neighbors, whereas a fully-implicit density-based solver will in general lead to a nonsymmetric system and thus requires more complex iterative solvers.

Modern computer codes for the solution of the MHD equations are mainly based on second or higher order Godunov-type finite volume schemes[41-50] or on the discontinuous Galerkin (DG) finite element framework.[49,51-56] In all these methods, the proper discretization of the magnetic field is of fundamental importance due to the well-known divergence-free constraint which the magnetic field must satisfy. Various solutions to this problem have been proposed in the literature so far and they can be essentially classified in two main categories: (i) the first class contains the exactly divergence-free methods, following the ideas of Balsara and Spicer[42,57] and which requires the electric field at the vertices of each element and thus a multi-dimensional Riemann solver[58-63]; (ii) the the second class uses divergence cleaning techniques, like either the Powell source term[64] based on the symmetric form of the MHD equations found by Godunov[65] or the hyperbolic generalized Lagrangian multiplier (GLM) approach of Munz et al[66] and Dedner et al.[67] The method proposed in this paper falls into the first class of exactly divergence-free schemes.

The rest of the paper is organized as follows: for the sake of simplicity and to facilitate the reader, we first present our new algorithm only for the ideal MHD equations in one space dimension, see Section 2. Computational results for the one-dimensional case are shown in Section 3. The extension of the method to the two-dimensional case, including viscous and resistive effects and a divergence-free evolution of the magnetic field is presented in Section 4. A set of classical benchmark problems for the ideal and VRMHD equations is then solved in Section 5, showing the performance of the method in the low Mach number limit as well as its robustness for shocked flows. Finally, in Section 6 we give some concluding remarks and an outlook to future work.

2 | NUMERICAL METHOD FOR THE IDEAL MHD EQUATIONS IN ONE SPACE DIMENSION

2.1 | Governing PDE

The ideal MHD equations in one space dimension read as follows:

$$\frac{\partial}{\partial t}\begin{pmatrix}\rho\\ \rho u\\ \rho v\\ \rho w\\ \rho E\\ B_x\\ B_y\\ B_z\end{pmatrix}+\frac{\partial}{\partial x}\begin{pmatrix}\rho u\\ \rho u^2+p+\frac{1}{8\pi}\mathbf{B}^2-\frac{1}{4\pi}B_x^2\\ \rho uv-\frac{1}{4\pi}B_xB_y\\ \rho uw-\frac{1}{4\pi}B_xB_z\\ u\left(\rho E+p+\frac{1}{8\pi}\mathbf{B}^2\right)-\frac{1}{4\pi}B_x(\mathbf{v}\cdot\mathbf{B})\\ 0\\ uB_y-vB_x\\ uB_z-wB_x\end{pmatrix}=0. \tag{1}$$

Here, time is denoted by $t \in \mathbb{R}_0^+$, whereas $x \in \Omega = [x_L, x_R] \subset \mathbb{R}$ is the spatial coordinate within the computational domain Ω. As usual, the fluid density and the fluid pressure are denoted by ρ and p, respectively; $\mathbf{v} = (u, v, w)$ is the velocity field and the magnetic field vector is $\mathbf{B} = (B_x, B_y, B_z)$; the total energy density is given by $\rho E = \rho e + \rho k + m = \rho e + \frac{1}{2}\rho\mathbf{v}^2 + \frac{1}{8\pi}\mathbf{B}^2$, where $\rho k = \frac{1}{2}\rho\mathbf{v}^2$ is the kinetic energy density of the fluid and $m = \frac{1}{8\pi}\mathbf{B}^2$ is the magnetic energy density; $e = e(p, \rho)$ is the specific internal energy per unit mass given by the so-called EOS, which is in general a nonlinear function of the fluid pressure and density. However, for an ideal gas, e and thus ρe are linear functions in p. In density-based Godunov-type finite volume schemes the EOS is typically required in the form $p = p(e, \rho)$, which can be obtained by solving the expression $e = e(p, \rho)$ for the pressure. Another important quantity that we will use in this paper is the so-called specific enthalpy, which is defined as $h = e + p/\rho$ and which allows to rewrite the first part of the flux for the total energy density as follows: $u(\rho E + p + m) = u(\rho k + 2m) + h(\rho u)$. The eight eigenvalues of the MHD system (1) are

$$\lambda_{1,8} = u \mp c_f, \quad \lambda_{2,7} = u \mp c_a, \quad \lambda_{3,6} = u \mp c_s, \quad \lambda_4 = u, \quad \lambda_5 = 0, \tag{2}$$

with

$$c_a = B_x/\sqrt{4\pi\rho}, \quad c_s^2 = \frac{1}{2}\left(b + c - \sqrt{(b+c)^2 - 4b_x c}\right), \quad c_f^2 = \frac{1}{2}\left(b + c + \sqrt{(b+c)^2 - 4b_x c}\right). \tag{3}$$

Here, c_a is the Alfvén wave speed, c_s is the speed of the slow magnetosonic waves, c_f is the one of the fast magnetosonic waves, and c is the adiabatic sound speed that can be computed from the equation of state $p = p(e, \rho)$ as $c^2 = \partial p/\partial\rho +$

$p/\rho^2 \partial p/\partial e$, which reduces to the well-known expression $c^2 = \gamma p/\rho$ for the ideal gas EOS. In the previous expressions, we have also used the abbreviations $b^2 = \mathbf{B}^2/(4\pi\rho)$ and $b_x = B_x/\sqrt{4\pi\rho}$. For a detailed discussion of the MHD equations and its eigenstructure, see the work of Roe and Balsara[68] and references therein. Similar to the compressible Euler equations, the crucial terms that give rise to the fast and slow magnetosonic wave speed c_f and c_s are the pressure term p_x in the momentum equation and the enthalpy term $(h\rho u)_x$ in the total energy equation. Therefore, these terms will have to be discretized *implicitly* in our semi-implicit numerical method in order to avoid a CFL condition based on the magnetosonic wave speeds c_f and c_s, whereas all remaining terms do not include the pressure and can therefore be discretized explicitly. In Section 2.3, we present a detailed discussion of the eigenvalues of an appropriately split MHD system in order to properly motivate our choice for discretizing certain terms explicitly and others implicitly. For a detailed analysis in the case of the compressible Euler and the shallow water equations, see the works of Casulli et al.[15,69]

2.2 | Ideal gas EOS

Our numerical scheme is presented for a general nonlinear equation of state $e = e(p, \rho)$. However, in order to compare with previously published results in the literature, we will use the ideal gas EOS for all numerical test problems reported later. The ideal gas EOS in the sought form $e = e(p, \rho)$ can be obtained from the so-called thermal equation of state $p = p(\rho, T)$ and the so-called caloric equation of state $e = e(T, \rho)$ by eliminating the temperature. For the ideal gas, the thermal and caloric equations of state take the well-known form

$$\frac{p}{\rho} = RT, \qquad \text{and} \qquad e = c_v T, \tag{4}$$

with the specific gas constant $R = c_p - c_v$, and the specific heat capacities c_v and c_p at constant volume and at constant pressure, respectively. From (4), one easily obtains

$$e = e(p, \rho) = \frac{p}{(\gamma - 1)\rho}, \tag{5}$$

which is linear in the pressure p and where $\gamma = c_p/c_v$ denotes the so-called ratio of specific heats. For more general cubic equations of state, the reader is referred to the famous work by Van der Waals[70] and more recent extensions.[71-73] For completely general equations of state for real fluids, see the works of Wagner et al.[74,75]

2.3 | Split form of the MHD system

Following the seminal paper of Toro and Vázquez[76] on the Euler equations, we now decide to *split* the flux of the MHD system (1) into a *convective-type* flux and a *pure pressure flux*, where the convective-type flux has to be understood in a more general sense in the MHD context due to the presence of the Alfvén waves. Note that the Toro and Vázquez (TV) splitting is substantially different from the flux vector splittings proposed in other works[77-79] since only in the TV splitting the resulting convective flux is totally free of any pressure terms. Writing PDE (1) formally as

$$\frac{\partial \mathbf{Q}}{\partial t} + \frac{\partial \mathbf{f}}{\partial x} = 0, \tag{6}$$

with $\mathbf{Q} = (\rho, \rho\mathbf{v}, \rho E, \mathbf{B})$ the vector of conservative variables and the flux vector $\mathbf{f}$ given in (1), we write the split system now as

$$\frac{\partial \mathbf{Q}}{\partial t} + \frac{\partial \mathbf{f}^c}{\partial x} + \frac{\partial \mathbf{f}^p}{\partial x} = 0, \tag{7}$$

with the convective-type flux $\mathbf{f}^c$ and the pure pressure flux $\mathbf{f}^p$ given as follows:

$$\mathbf{f}^c(\mathbf{Q}) = \begin{pmatrix} \rho u \\ \rho u^2 + m - \frac{1}{4\pi}B_x^2 \\ \rho uv - \frac{1}{4\pi}B_x B_y \\ \rho uw - \frac{1}{4\pi}B_x B_z \\ u(\rho k + 2m) - \frac{1}{4\pi}B_x(\mathbf{v}\cdot\mathbf{B}) \\ 0 \\ uB_y - vB_x \\ uB_z - wB_x \end{pmatrix}, \qquad \mathbf{f}^p(\mathbf{Q}) = \begin{pmatrix} 0 \\ p \\ 0 \\ 0 \\ h\rho u \\ 0 \\ 0 \\ 0 \end{pmatrix}. \tag{8}$$

Recall that we have $h = e(p,\rho) + p/\rho$ and $m = \frac{1}{8\pi}\mathbf{B}^2$ as well as $\rho k = \frac{1}{2}\rho\mathbf{v}^2$ according to the definitions in Section 2.1. It is obvious that $\mathbf{f}^c$ does not contain any contribution of the pressure p, whereas $\mathbf{f}^p$ involves *only* the density ρ, the pressure p and the velocity component u and does *not* involve any contribution from the magnetic field. In this sense, our new splitting is the closest possible to the TV splitting since our pressure system is exactly the same as the one obtained by Toro and Vázquez.[76] Note in particular also that the split form (7) with (8) chosen in this paper is *different* from all splittings of the MHD system proposed in Balsara et al.[80] It is easy to check that the convective subsystem

$$\partial_t \mathbf{Q} + \partial_x \mathbf{f}^c = 0 \tag{9}$$

has the following eigenvalues

$$\lambda^c_{1,8} = u \mp \sqrt{\frac{\mathbf{B}^2}{4\pi\rho}}, \qquad \lambda^c_{2,7} = u \mp \frac{B_x}{\sqrt{4\pi\rho}}, \qquad \lambda^c_{3,4} = 0, \qquad \lambda^c_{5,6} = u, \tag{10}$$

whereas our pressure subsystem

$$\partial_t \mathbf{Q} + \partial_x \mathbf{f}^p = 0 \tag{11}$$

is *identical* to the Toro and Vázquez pressure system and therefore has the eigenvalues

$$\lambda^p_1 = \frac{1}{2}\left(u - \sqrt{u^2+4c^2}\right), \qquad \lambda^p_{2,3,4,5,6,7} = 0, \qquad \lambda^p_8 = \frac{1}{2}\left(u + \sqrt{u^2+4c^2}\right), \tag{12}$$

ie, the pressure subsystem is *always* subsonic, independent of $\mathbf{B}$. With subsonic we mean here that there is always one negative eigenvalue $\lambda^p_1 < 0$, a multiple zero eigenvalue and one positive eigenvalue $\lambda^p_8 > 0$. Recall that for the ideal gas EOS, we have $c^2 = \gamma p/\rho$. Looking at the eigenvalues (12) of the pressure subsystem, it becomes obvious that for low Mach number flows, ie, when the ratio $M = u/c \ll 1$, or even more in the incompressible limit when $M \to 0$, the terms appearing in the pressure subsystem need to be discretized *implicitly*, whereas the eigenvalues of the convective subsystem (10) suggest that an *explicit* discretization of the convective subsystem is still possible unless the Alfvén speed c_a gets large, eg, because the magnitude of the magnetic field $\|\mathbf{B}\|$ gets large or because the density gets low. In the latter case, also the magnetic field needs to be discretized implicitly, but this is not the scope of the present paper.

2.4 | Semi-implicit discretization on a staggered grid

The ideal MHD Equations (1) are discretized on a *staggered* grid, which is typical for semi-implicit schemes applied to the incompressible Navier-Stokes and shallow water equations.[1,9] In the staggered grid, the *primary* control volumes are the intervals $\Omega_i = [x_{i-\frac{1}{2}}, x_{i+\frac{1}{2}}]$ of length $\Delta x_i = x_{i+\frac{1}{2}} - x_{i-\frac{1}{2}}$ with barycenters located in $x_i = \frac{1}{2}(x_{i-\frac{1}{2}} + x_{i+\frac{1}{2}})$. The number of primary control volumes is denoted by N_x. The $N_x + 1$ *dual* control volumes are $\Omega_{i+\frac{1}{2}} = [x_i, x_{i+1}]$ with the associated mesh spacing $\Delta x_{i+\frac{1}{2}} = x_{i+1} - x_i = \frac{1}{2}(\Delta x_i + \Delta x_{i+1})$. The entire nonlinear convective subsystem (9) will be discretized on the primary control volumes, whereas the pressure subsystem (11) is discretized as usual on the combination of the two staggered grids, defining the discrete pressure p^n_i in the centers of the primary cells Ω_i, whereas the discrete velocity $u^n_{i+\frac{1}{2}}$ in the pressure system is located at the cell boundaries. In order to combine the discretization of the convective subsystem on the main grid with the discretization of the pressure subsystem on the staggered mesh, we will need to *average* quantities from the main grid to the dual grid and vice versa. This is simply obtained by the following conservative averaging operators:

$$\mathbf{Q}^n_i = \frac{1}{2}\left(\mathbf{Q}^n_{i-\frac{1}{2}} + \mathbf{Q}^n_{i+\frac{1}{2}}\right), \qquad \mathbf{Q}^n_{i+\frac{1}{2}} = \frac{1}{2}\frac{1}{\Delta x_{i+\frac{1}{2}}}\left(\Delta x_i \mathbf{Q}^n_i + \Delta x_{i+1}\mathbf{Q}^n_{i+1}\right). \tag{13}$$

At this point, we would like to emphasize that the use of a staggered grid arrangement is necessary for the implicit part of the algorithm in order to obtain a final pressure system that is symmetric and positive definite and that has a computational stencil that involves only the cell itself and its direct edge neighbors.

2.4.1 | Convective subsystem

The convective terms collected in $\mathbf{f}^c$ are now discretized on the main grid using a standard *explicit* first- or second-order accurate finite volume scheme of the form

$$\mathbf{Q}^*_i = \mathbf{Q}^n_i - \frac{\Delta t}{\Delta x_i}\left(\mathbf{f}^c_{i+\frac{1}{2}} - \mathbf{f}^c_{i-\frac{1}{2}}\right), \tag{14}$$

which yields the intermediate state vector $\mathbf{Q}_i^*$ that does not yet contain the contribution of the pressure terms. Throughout this paper, we employ the simple Rusanov-type flux

$$\mathbf{f}^c_{i+\frac{1}{2}} = \frac{1}{2}\left(\mathbf{f}^c\left(\mathbf{Q}^+_{i+\frac{1}{2}}\right) + \mathbf{f}^c\left(\mathbf{Q}^-_{i+\frac{1}{2}}\right)\right) - \frac{1}{2}s_{\max}\left(\mathbf{Q}^+_{i+\frac{1}{2}} - \mathbf{Q}^-_{i+\frac{1}{2}}\right), \tag{15}$$

where $\mathbf{Q}^-_{i+\frac{1}{2}}$ and $\mathbf{Q}^+_{i+\frac{1}{2}}$ denote the left and right boundary extrapolated states at the cell interface $x_{i+\frac{1}{2}}$ and $s_{\max} = \max_l(|\lambda^c_l(\mathbf{Q}^-_{i+\frac{1}{2}})|, |\lambda^c_l(\mathbf{Q}^+_{i+\frac{1}{2}})|)$ is the maximum signal speed of the convective subsystem at the interface. For a first-order scheme, one simply has $\mathbf{Q}^-_{i+\frac{1}{2}} = \mathbf{Q}^n_i$ and $\mathbf{Q}^+_{i+\frac{1}{2}} = \mathbf{Q}^n_{i+1}$, whereas a second-order MUSCL-Hancock-type TVD scheme is obtained by setting $\mathbf{Q}^-_{i+\frac{1}{2}} = \mathbf{w}_i(x_{i+\frac{1}{2}}, t^{n+\frac{1}{2}})$ and $\mathbf{Q}^+_{i+\frac{1}{2}} = \mathbf{w}_{i+1}(x_{i+\frac{1}{2}}, t^{n+\frac{1}{2}})$, where $\mathbf{w}_i(x,t)$ is a space-time polynomial reconstruction of the state vector in each cell Ω_i that reads

$$\mathbf{w}_i(x,t) = \mathbf{Q}^n_i + \frac{\Delta\mathbf{Q}^n_i}{\Delta x_i}(x - x_i) + \partial_t\mathbf{Q}^n_i(t - t^n). \tag{16}$$

The space-time expansion coefficients in (16) are given by

$$\frac{\Delta\mathbf{Q}^n_i}{\Delta x_i} = \text{minmod}\left(\frac{\mathbf{Q}^n_{i+1} - \mathbf{Q}^n_i}{\Delta x_{i+\frac{1}{2}}}, \frac{\mathbf{Q}^n_i - \mathbf{Q}^n_{i-1}}{\Delta x_{i-\frac{1}{2}}}\right), \partial_t\mathbf{Q}^n_i = \frac{\mathbf{f}^c\left(\mathbf{Q}^n_i - \frac{1}{2}\Delta\mathbf{Q}^n_i\right) - \mathbf{f}^c\left(\mathbf{Q}^n_i + \frac{1}{2}\Delta\mathbf{Q}^n_i\right)}{\Delta x_i}, \tag{17}$$

with the usual minmod slope limiter function.[25] Since the mass conservation equation and the PDE for the transverse momentum in y and z direction do not contain the pressure, we can immediately set $\rho^{n+1}_i = \rho^*_i$, $(\rho v)^{n+1}_i = (\rho v)^*_i$ and $(\rho w)^{n+1}_i = (\rho w)^*_i$. In one space dimension, no divergence-free treatment of the magnetic field is necessary, and therefore, we also have $\mathbf{B}^{n+1}_i = \mathbf{B}^*_i$. This completes the description of the explicit part of the scheme.

2.4.2 | Pressure subsystem

The pressure subsystem involves only the x-momentum equation and the total energy equation. The *semi-implicit* discretization of the x-momentum equation reads

$$(\rho u)^{n+1}_{i+\frac{1}{2}} = (\rho u)^*_{i+\frac{1}{2}} - \frac{\Delta t}{\Delta x_{i+\frac{1}{2}}}\left(p^{n+1}_{i+1} - p^{n+1}_i\right), \tag{18}$$

where the pressure is now taken *implicitly*, whereas the *explicit* operator for the discretization of the nonlinear convective terms, ie, for the computation of $(\rho u)^*_{i+\frac{1}{2}}$ has been detailed previously. Note that $(\rho u)^*_{i+\frac{1}{2}}$ is located on the dual mesh and therefore has to be averaged from the main grid to the dual mesh via (13). According to a previous work,[30] a *preliminary* discretization of the total energy equation is now chosen as follows:

$$\Delta x_i\left(\rho^{n+1}_i e\left(p^{n+1}_i, \rho^{n+1}_i\right) + \frac{1}{2}\left((\tilde{\rho k})^{n+1}_{i-\frac{1}{2}} + (\tilde{\rho k})^{n+1}_{i+\frac{1}{2}}\right) + m^{n+1}_i\right) = \Delta x_i(\rho E)^*_i - \Delta t\left(\tilde{h}^{n+1}_{i+\frac{1}{2}}(\rho u)^{n+1}_{i+\frac{1}{2}} - \tilde{h}^{n+1}_{i-\frac{1}{2}}(\rho u)^{n+1}_{i-\frac{1}{2}}\right). \tag{19}$$

The tilde symbols indicate that a further discretization step is necessary that will be explained later. Inserting the discrete momentum Equation (18) into the discrete energy Equation (19) and using $m^{n+1}_i = m^*_i$ yield the following *preliminary* system for the unknown pressure:

$$\begin{aligned}\Delta x_i\rho^{n+1}_i e\left(p^{n+1}_i, \rho^{n+1}_i\right) - \Delta t^2\left(\frac{\tilde{h}^{n+1}_{i+\frac{1}{2}}}{\Delta x_{i+\frac{1}{2}}}\left(p^{n+1}_{i+1} - p^{n+1}_i\right) - \frac{\tilde{h}^{n+1}_{i-\frac{1}{2}}}{\Delta x_{i-\frac{1}{2}}}\left(p^{n+1}_i - p^{n+1}_{i-1}\right)\right) = \\ \Delta x_i\left((\rho E)^*_i - m^*_i - \frac{1}{2}\left((\tilde{\rho k})^{n+1}_{i-\frac{1}{2}} + (\tilde{\rho k})^{n+1}_{i+\frac{1}{2}}\right)\right) - \Delta t\left(\tilde{h}^{n+1}_{i+\frac{1}{2}}(\rho u)^*_{i+\frac{1}{2}} - \tilde{h}^{n+1}_{i-\frac{1}{2}}(\rho u)^*_{i-\frac{1}{2}}\right),\end{aligned} \tag{20}$$

which has exactly the same structure as the one obtained in the previous work[30] for the compressible Euler equations. Therefore, following the same reasoning as explained in the same work,[30] the quantities marked with a tilde symbol cannot be discretized directly at the new time t^{n+1} since, in this case, the resulting pressure system would become strongly nonlinear and difficult to control. To circumvent the problem, we employ a simple *Picard iteration*, as suggested in Casulli and Zanolli.[39] The Picard iteration index will be denoted by r in the following. This yields the following iterative scheme,

which requires only the solution of the following *mildly nonlinear* system for the pressure $p_i^{n+1,r+1}$ at each Picard iteration

$$\Delta x_i \rho e\left(p_i^{n+1,r+1}\right) - \Delta t^2 \left(\frac{h_{i+\frac{1}{2}}^{n+1,r}}{\Delta x_{i+\frac{1}{2}}} \left(p_{i+1}^{n+1,r+1} - p_i^{n+1,r+1}\right) - \frac{h_{i-\frac{1}{2}}^{n+1,r}}{\Delta x_{i-\frac{1}{2}}} \left(p_i^{n+1,r+1} - p_{i-1}^{n+1,r+1}\right) \right) = b_i^r, \tag{21}$$

with the abbreviation $\rho e(p_i^{n+1,r+1}) = \rho_i^{n+1} e(p_i^{n+1,r+1}, \rho_i^{n+1})$ and the known right-hand side

$$b_i^r = \Delta x_i \left((\rho E)_i^* - m_i^* - \frac{1}{2} \left((\rho k)_{i-\frac{1}{2}}^{n+1,r} + (\rho k)_{i+\frac{1}{2}}^{n+1,r} \right) \right) - \Delta t \left(h_{i+\frac{1}{2}}^{n+1,r} (\rho u)_{i+\frac{1}{2}}^* - h_{i-\frac{1}{2}}^{n+1,r} (\rho u)_{i-\frac{1}{2}}^* \right). \tag{22}$$

Note that the density $\rho_i^{n+1} = \rho_i^*$ and the magnetic energy $m_i^{n+1} = m_i^*$ are already known from the explicit discretization (14); hence, in (21), the new pressure is the only unknown. Using a more compact notation, the above system (21) can be written as follows:

$$\boldsymbol{\rho}\mathbf{e}(\mathbf{p}^{n+1,r+1}) + \mathbf{T}^r \mathbf{p}^{n+1,r+1} = \mathbf{b}^r, \tag{23}$$

with the vector of the unknowns $\mathbf{p}^{n+1,r+1} = (p_1^{n+1,r+1}, \dots, p_i^{n+1,r+1}, \dots, p_{N_x}^{n+1,r+1})$. The vector $\mathbf{b}^r$ contains the known right-hand side of (21). Matrix $\mathbf{T}^r$ is symmetric and at least positive semidefinite and takes into account the linear part of the system, whereas the nonlinearity is contained in the vector function $\boldsymbol{\rho}\mathbf{e}(\mathbf{p}^{n+1,r+1}) = (\Delta x_1 \rho_1^{n+1} e(p_1^{n+1,r+1}, \rho_1^{n+1}), \dots, \Delta x_i \rho_i^{n+1} e(p_i^{n+1,r+1}, \rho_i^{n+1}), \dots, \Delta x_{N_x} \rho_{N_x}^{n+1} e(p_{N_x}^{n+1,r+1}, \rho_{N_x}^{n+1}))$, which means a componentwise evaluation of the internal energy density in terms of pressure and density. We stress again that the density ρ_i^{n+1} at the new time level is already known from (14), ie, for the solution of the mildly nonlinear system, the equation of state can be considered as a function of pressure alone, with a given density.

The time step, the mesh spacings, and the enthalpy h are nonnegative quantities, and we suppose that the specific internal energy $e(p, \rho)$ is a non-negative, non-decreasing function whose derivative w.r.t. the pressure is a nonnegative function of bounded variation. Thanks to the semi-implicit discretization of the pressure subsystem on the staggered mesh, the matrix $\mathbf{T}^r$ in system (21) is *symmetric* and at least *positive semi-definite*, which is quite a remarkable property, considering the complex structure of the MHD system (1). It is therefore possible to employ the same (nested) Newton-type techniques for the solution of (23) as those proposed and analyzed by Casulli et al.[37-40] For all implementation details and a rigorous convergence proof of the (nested) Newton method, the reader is referred to the above references. The iterative Newton-type techniques of Casulli et al have already been used with great success as building block of semi-implicit finite volume schemes in different application contexts, see other works.[13,14,81-85] Due to the properties of $\mathbf{T}^r$, the linear subproblems within the Newton-type algorithm can be solved at the aid of a matrix-free conjugate gradient method or with the Thomas algorithm for tridiagonal systems in the one-dimensional case. Note that, for the ideal gas EOS, the resulting system (23) becomes *linear* in the pressure; hence, one single Newton iteration is sufficient to solve (23). From the new pressure $p_i^{n+1,r+1}$, the momentum density at the next Picard iteration can be obtained as

$$(\rho u)_{i+\frac{1}{2}}^{n+1,r+1} = (\rho u)_{i+\frac{1}{2}}^* - \frac{\Delta t}{\Delta x_{i+\frac{1}{2}}} \left(p_{i+1}^{n+1,r+1} - p_i^{n+1,r+1}\right). \tag{24}$$

The new pressure and momentum are both needed to update the enthalpies at the element interfaces as well as the kinetic energy contribution to the total energy at the new time level. As already observed in previous works,[30,39] it is sufficient to carry out only very few Picard iterations to obtain a satisfactory solution. In all test problems presented in this paper, we stop the Picard process after $r_{\max} = 2$ iterations. At the end of the last Picard iteration, we set $p_i^{n+1} = p_i^{n+1,r+1}$, $(\rho u)_{i+\frac{1}{2}}^{n+1} = (\rho u)_{i+\frac{1}{2}}^{n+1,r+1}$, $h_{i+\frac{1}{2}}^{n+1} = h_{i+\frac{1}{2}}^{n+1,r+1}$ and update the total energy density using the conservative formula

$$(\rho E)_i^{n+1} = (\rho E)_i^* - \frac{\Delta t}{\Delta x_i} \left(h_{i+\frac{1}{2}}^{n+1} (\rho u)_{i+\frac{1}{2}}^{n+1} - h_{i-\frac{1}{2}}^{n+1} (\rho u)_{i-\frac{1}{2}}^{n+1} \right). \tag{25}$$

Finally, in order to proceed with the next time step, we still need to average the momentum back from the staggered mesh to the main grid by using the averaging operator (13) from the dual mesh to the main grid.

From (14), (18), and (25), it is obvious that the scheme is written in a conservative flux form for all conservation equations and the averaging operators between main and dual grid are also conservative; hence, the proposed method is locally and globally conservative for mass, momentum, and total energy. For this reason, the method is able to handle flows with very strong shocks properly, as shown via several numerical test problems in the next section. Its stability is only restricted by a *mild CFL condition* based on the eigenvalues of the convective subsystem λ_l^c and is *not* based on the speed of the magnetosonic waves c_s and c_f. This makes the method particularly well suited for the discretization of *low*

Mach number flows, as long as the ratio of Alfvén speed to fast magnetosonic wavespeed c_a/c_f is small or at most of the order of the flow velocity. For large Alfvén speeds c_a, the present method is *not* efficient, and the magnetic field needs to be discretized implicitly.

2.4.3 | Equivalent fully discrete one-step FV scheme

Since our staggered semi-implicit finite volume method is conservative, it can also be written in an equivalent fully discrete one-step flux form that is given in this section. However, we stress that, in practice, the scheme is implemented as discussed in the previous sections and *not* in the form presented here. We give the fully discrete one-step form only for the sake of completeness, assuming a uniform grid spacing Δx to ease notation. Inserting the definition of the star quantities $\mathbf{Q}_i^*$ into (18) and making use of the conservative averaging operators (13), after some calculations, one can write the discrete momentum equation in x direction equivalently as

$$(\rho u)_i^{n+1} = (\rho u)_i^n - \frac{\Delta t}{\Delta x}\left(\tilde{f}^{\rho u}_{i+\frac{1}{2}} - \tilde{f}^{\rho u}_{i-\frac{1}{2}}\right), \tag{26}$$

with the numerical momentum flux

$$\tilde{f}^{\rho u}_{i+\frac{1}{2}} = \frac{1}{4}\left(f^{c,\rho u}_{i-\frac{1}{2}} + 2 f^{c,\rho u}_{i+\frac{1}{2}} + f^{c,\rho u}_{i+\frac{3}{2}}\right) - \frac{1}{4}\frac{\Delta x}{\Delta t}\left((\rho u)^n_{i+1} - (\rho u)^n_i\right) + \frac{1}{2}\left(p^{n+1}_i + p^{n+1}_{i+1}\right). \tag{27}$$

Here, $f^{c,\rho u}_{i+\frac{1}{2}}$ denotes the numerical flux component for the variable ρu in the flux vector $\mathbf{f}^c_{i+\frac{1}{2}}$ used in Equation (14). It is obvious from (27) that this is *not* a simple two-point flux, as it is used in standard Godunov-type finite volume methods. The term in the second bracket represents an additional numerical viscosity that comes from the averaging to the dual staggered grid and back. It is similar to the numerical viscosity in the FORCE scheme of Toro and Billet and its extensions, see other works,[86-88] where also an averaging procedure of the conservation law onto a dual edge-based staggered mesh is employed. The fully discrete energy Equation (25) can be written as

$$(\rho E)_i^{n+1} = (\rho E)_i^n - \frac{\Delta t}{\Delta x}\left(\tilde{f}^{\rho E}_{i+\frac{1}{2}} - \tilde{f}^{\rho E}_{i-\frac{1}{2}}\right), \tag{28}$$

with the numerical energy flux

$$\tilde{f}^{\rho E}_{i+\frac{1}{2}} = f^{c,\rho E}_{i+\frac{1}{2}} + h^{n+1}_{i+\frac{1}{2}}(\rho u)^{n+1}_{i+\frac{1}{2}}, \tag{29}$$

where

$$(\rho u)^{n+1}_{i+\frac{1}{2}} = \frac{1}{2}\left(\rho u^n_i + (\rho u)^n_{i+1}\right) - \frac{1}{2}\frac{\Delta t}{\Delta x}\left(f^{c,\rho u}_{i+\frac{3}{2}} - f^{c,\rho u}_{i-\frac{1}{2}}\right) - \frac{\Delta t}{\Delta x}\left(p^{n+1}_{i+1} - p^{n+1}_i\right). \tag{30}$$

The discrete mass conservation equation is already given by (14), since $\rho_i^{n+1} = \rho_i^*$. The same Equation (14) holds for the transverse velocity components v and w and in one space dimension it holds as well for the magnetic field.

3 | NUMERICAL RESULTS IN 1D

In this section, we apply our new semi-implicit finite volume scheme to a set of Riemann problems of the ideal MHD equations, some of which have been introduced and analyzed in other works.[89-92] The eigenstructure of the ideal MHD equations has been discussed in Roe and Balsara,[68] whereas the exact Riemann solver used for the comparisons presented in this paper has kindly been provided by Falle and Komissarov.[93,94] For an alternative exact Riemann solver of the MHD equations, see the work of Torrilhon.[95] In all our tests, we use a computational domain $\Omega = [-0.5, +0.5]$ that is discretized at the aid of 1000 pressure control volumes (apart from RP0, for which only 100 points have been used), which is only slightly more than the typical resolution of 800 elements chosen for the explicit finite volume schemes used in.[95-97] In RP1-RP4 the Courant number is set to CFL $= 0.9$, based on the maximum eigenvalues of the convective subsystem and a second order MUSCL-type TVD scheme is used for the discretization of the explicit terms. For RP0, we use a constant time step size of $\Delta t = 0.1$. The initial condition for all Riemann problems consists in a constant left and right state that are separated by a discontinuity located at x_d. The initial data as well as the value for x_d are reported in Table 1. The ratio of specific heats is $\gamma = \frac{5}{3}$ for all cases. The comparison between the numerical solution obtained with the new SIFV scheme and the exact solution is presented in Figures 1-5. The first Riemann problem (RP0) is just a sanity check in order to verify that our new SIFV method is able to resolve isolated steady contact waves without magnetic field exactly. This property follows trivially from the chosen discretization and is also confirmed in our numerical experiments, see Figure 1.

TABLE 1 Initial states left and right for the density ρ, velocity vector $\mathbf{v} = (u, v, w)$, the pressure p and the magnetic field vector $\mathbf{B} = (B_x, B_y, B_z)$ for the Riemann problems of the ideal classical magnetohydrodynamics equations. In all cases $\gamma = 5/3$. The initial position of the discontinuity is $x_d = 0$ for RP0, RP1, and RP4, whereas it is $x_d = -0.1$ for RP2 and RP3

Case	ρ	u	v	w	p	B_x	B_y	B_z
RP0 L:	1.0	0.0	0.0	0.0	1.0	0.0	0.0	0.0
R:	0.125	0.0	0.0	0.0	1.0	0.0	0.0	0.0
RP1 L:	1.0	0.0	0.0	0.0	1.0	$\frac{3}{4}\sqrt{4\pi}$	$\sqrt{4\pi}$	0.0
R:	0.125	0.0	0.0	0.0	0.1	$\frac{3}{4}\sqrt{4\pi}$	$-\sqrt{4\pi}$	0.0
RP2 L:	1.08	1.2	0.01	0.5	0.95	2.0	3.6	2.0
R:	0.9891	-0.0131	0.0269	0.010037	0.97159	2.0	4.0244	2.0026
RP3 L:	1.7	0.0	0.0	0.0	1.7	3.899398	3.544908	0.0
R:	0.2	0.0	0.0	-1.496891	0.2	3.899398	2.785898	2.192064
RP4 L:	1.0	0.0	0.0	0.0	1.0	$1.3\sqrt{4\pi}$	$\sqrt{4\pi}$	0.0
R:	0.4	0.0	0.0	0.0	0.4	$1.3\sqrt{4\pi}$	$-\sqrt{4\pi}$	0.0

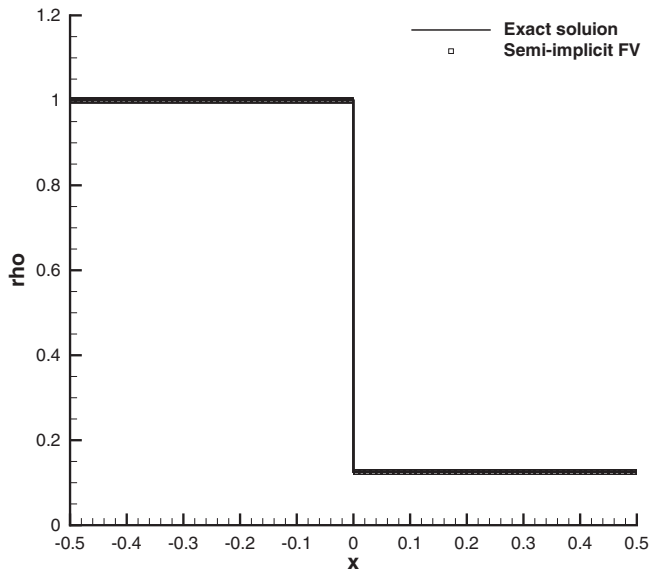

FIGURE 1 Exact and numerical solution for Riemann problem RP0 (isolated steady contact wave) solving the ideal magnetohydrodynamics equations with the new semi-implicit finite volume (FV) scheme. The density is shown at a final time of $t = 10$, confirming that our scheme is able to preserve steady contact waves exactly

Riemann problem (RP1) is the one of Brio and Wu,[89] for which it is well known that all standard finite volume schemes produce a compound wave instead of the wave pattern suggested by the exact Riemann solver. Only the random choice method of Glimm[98] was able to reproduce the correct solution in this case, as discussed in the work of Falle and Komissarov.[93] Therefore, despite the disagreement with the exact solution in the density profile, our numerical results are in line with others published in the literature. Furthermore, the numerical results obtained for the magnetic field component B_y agree well with the exact solution. The second Riemann problem (RP2) goes back to Ryu and Jones[90] and presents a wave pattern composed of discontinuities in all seven waves of the MHD system. The agreement between our numerical solution and the exact solution is very good in this case. In addition, problem RP3 contains seven waves, but compared to RP2, the two left waves are rarefactions and not shocks. Moreover, in this case, the semi-implicit finite volume scheme is able to capture the wave pattern properly, apart from the weak right-moving shock. In the last Riemann problem (RP4), our scheme has some difficulties in capturing the second wave from the left at the given grid resolution, but this behavior is similar to what was also observed in previous works.[92,99] The profile of the magnetic field component B_y is well reproduced in this case.

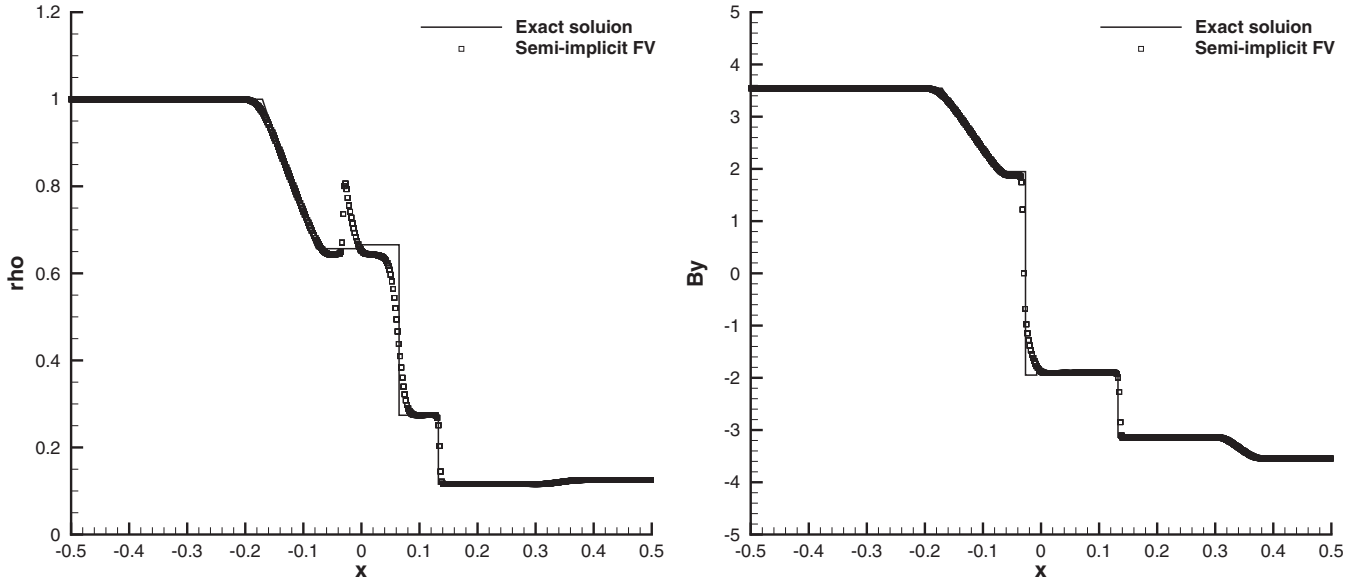

FIGURE 2 Exact and numerical solution for Riemann problem RP1 solving the ideal magnetohydrodynamics equations with the new semi-implicit finite volume (FV) scheme. Density (left) and magnetic field component B_y (right) at time $t = 0.1$

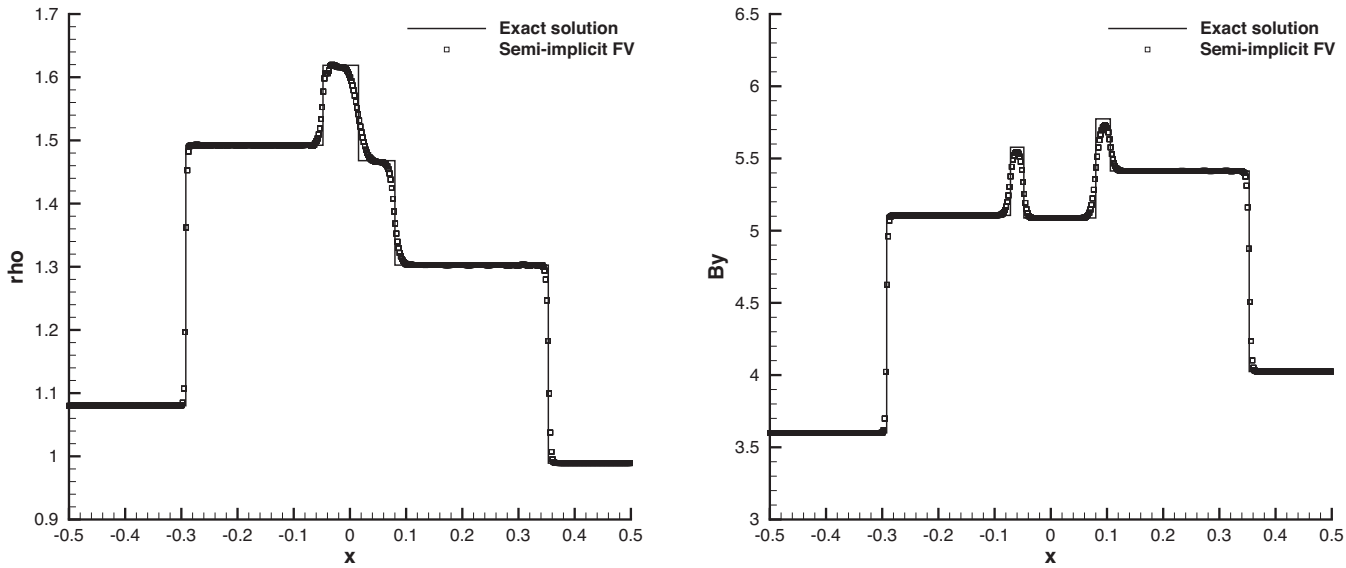

FIGURE 3 Exact and numerical solution for Riemann problem RP2 solving the ideal magnetohydrodynamics equations with the new semi-implicit finite volume (FV) scheme. Density (left) and magnetic field component B_y (right) at time $t = 0.2$

Overall, we can conclude that the numerical results obtained with our new algorithm are in line with those previously published in the literature. However, at this point, it is important to stress that our semi-implicit finite volume scheme is a so-called *pressure-based* solver, which is particularly tailored to work in the low Mach number regime or even in the incompressible limit of the equations, whereas all standard explicit finite volume schemes that are typically used for the solution of the MHD equations are so-called *density-based* methods, which are unable to deal with the incompressible limit of the equations. It is therefore quite remarkable to observe that the new pressure-based semi-implicit method performs almost as well as standard Godunov-type schemes in this set of Riemann problems. Encouraged by these results, in the next section, we now present the extension to the viscous and resistive case in two space dimensions, where particular care needs to be taken in order to obtain an exactly divergence-free formulation of the scheme.

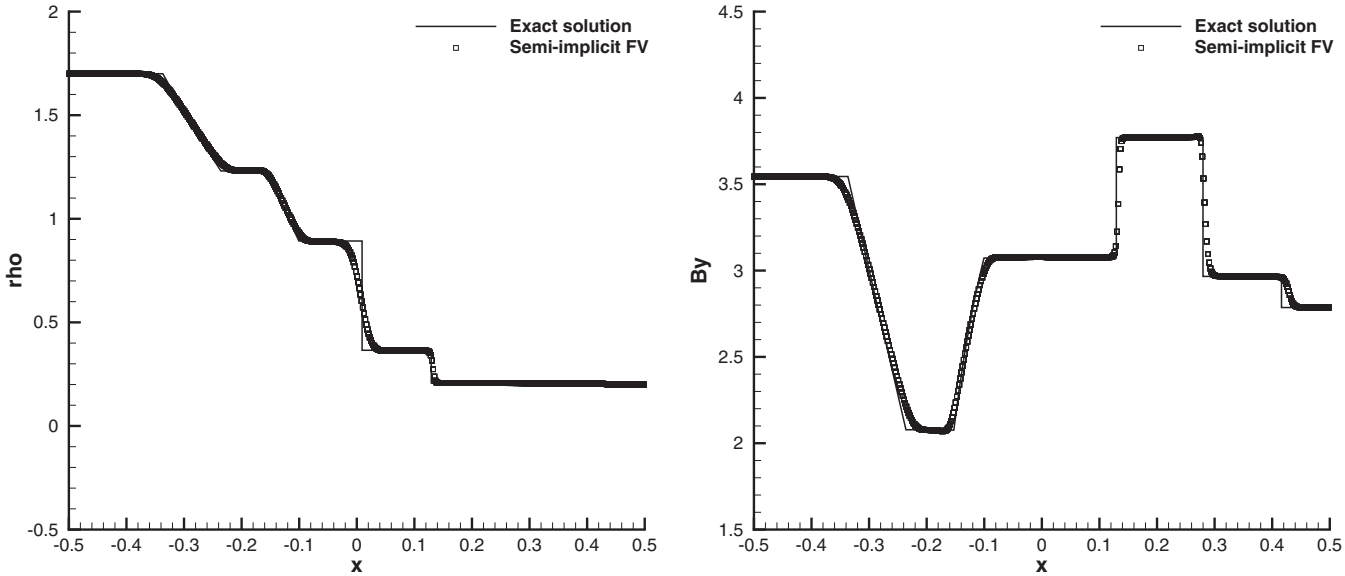

FIGURE 4 Exact and numerical solution for Riemann problem RP3 solving the ideal magnetohydrodynamics equations with the new semi-implicit finite volume (FV) scheme. Density (left) and magnetic field component B_y (right) at time $t = 0.15$

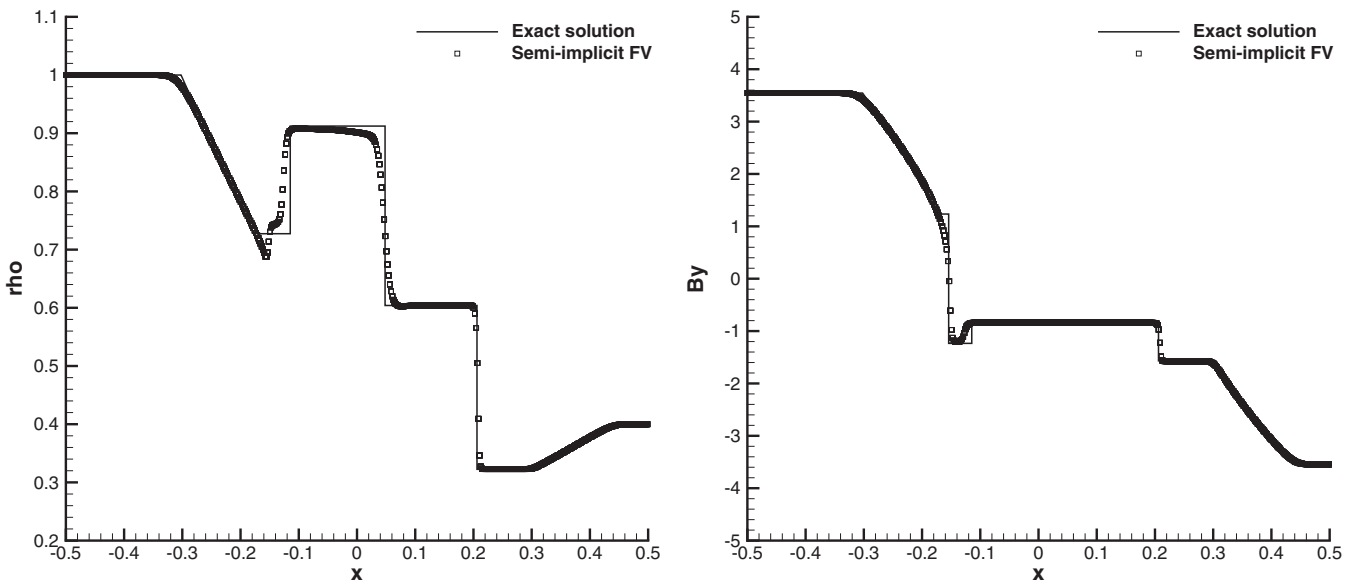

FIGURE 5 Exact and numerical solution for Riemann problem RP4 solving the ideal magnetohydrodynamics equations with the new semi-implicit finite volume (FV) scheme. Density (left) and magnetic field component B_y (right) at time $t = 0.16$

4 | EXTENSION TO VISCOUS FLOWS IN MULTIPLE SPACE DIMENSIONS

4.1 | Governing equations

In multiple space dimensions, the VRMHD equations read

$$\frac{\partial}{\partial t}\begin{pmatrix}\rho\\ \rho\mathbf{v}\\ \rho E\\ \mathbf{B}\end{pmatrix}+\nabla\cdot\begin{pmatrix}\rho\mathbf{v}\\ \rho\mathbf{v}\otimes\mathbf{v}+\left(p+\frac{\mathbf{B}^2}{8\pi}\right)\mathbf{I}-\frac{1}{4\pi}\mathbf{B}\otimes\mathbf{B}\\ \mathbf{v}^T\left(\rho E+p+\frac{1}{8\pi}\mathbf{B}^2\right)-\frac{1}{4\pi}\mathbf{v}^T\mathbf{B}\otimes\mathbf{B}\\ \mathbf{B}\otimes\mathbf{v}-\mathbf{v}\otimes\mathbf{B}\end{pmatrix}=\nabla\cdot\mathbf{F}_v, \tag{31}$$

with the identity matrix $\mathbf{I}$ and the viscous flux tensor $\mathbf{F}^v = (\mathbf{f}^v, \mathbf{g}^v)$ defined as

$$\mathbf{F}^v(\mathbf{V}, \nabla\mathbf{V}) = \begin{pmatrix} 0 \\ \mu\left(\nabla\mathbf{v} + \nabla\mathbf{v}^T - \frac{2}{3}(\nabla\cdot\mathbf{v})\mathbf{I}\right) \\ \mu\mathbf{v}^T\left(\nabla\mathbf{v} + \nabla\mathbf{v}^T - \frac{2}{3}(\nabla\cdot\mathbf{v})\mathbf{I}\right) + \lambda\nabla T + \frac{\eta}{4\pi}\mathbf{B}^T\left(\nabla\mathbf{B} - \nabla\mathbf{B}^T\right) \\ \eta\left(\nabla\mathbf{B} - \nabla\mathbf{B}^T\right) \end{pmatrix}. \tag{32}$$

Here, $\mathbf{Q} = (\rho, \rho\mathbf{v}, \rho E, \mathbf{B})$ and $\mathbf{V} = (\rho, \mathbf{v}, T, \mathbf{B})$ are the vectors of conserved and primitive variables, respectively, T is the temperature given by the thermal equation of state $T = T(p, \rho)$, μ is the kinematic viscosity, λ is the thermal conductivity, and η is the electric resistivity of the fluid. The Prandtl number is defined as $Pr = \mu\gamma c_v/\lambda$. It is interesting to note that, for the MHD system in two and three space dimensions, the number of variables contained in the vectors of conserved and primitive quantities $\mathbf{Q}$ and $\mathbf{V}$ does not increase with respect to the one-dimensional case, whereas the number of independent coordinate directions obviously increases. In order to extend our new semi-implicit scheme to the ideal and to the VRMHD equations in multiple space dimensions, special care must be taken concerning the $\nabla\cdot\mathbf{B} = 0$ constraint, ie, the divergence of the magnetic field must remain zero for all times if it was initially zero. Several strategies have been developed in the literature in the past to satisfy the divergence constraint exactly or approximately, see, eg, the well-known divergence-free schemes for MHD of Balsara and Spicer[57] and subsequent work by Balsara,[42,58,59] the discretization proposed by Powell et al[45,64] based on the symmetric hyperbolic form of the MHD equations found by Godunov,[65] or the hyperbolic divergence-cleaning approach of Munz et al[66] and Dedner et al.[67] Since we already use a staggered mesh for the semi-implicit discretization of the pressure subsystem, it is very natural to employ the strategy of Balsara and Spicer,[42,57] which also adopts a staggered mesh for the time evolution of the magnetic field. In this paper, we properly extend this technique to deal also with the resistive terms. For that purpose, it has to be noted that, with $\nabla\cdot\mathbf{B} = 0$, the resistive term can be rewritten in terms of a double curl operator as $\eta\nabla\cdot(\nabla\mathbf{B} - \nabla\mathbf{B}^T) = -\eta\nabla\times\nabla\times\mathbf{B}$, and therefore, the induction equation for the magnetic field reads

$$\frac{\partial\mathbf{B}}{\partial t} + \nabla\times\mathbf{E} = 0, \tag{33}$$

with the electric field vector given by

$$\mathbf{E} = -\mathbf{v}\times\mathbf{B} + \eta\nabla\times\mathbf{B}, \tag{34}$$

which reduces to the standard expression $\mathbf{E} = -\mathbf{v}\times\mathbf{B}$ for the ideal MHD equations ($\eta = 0$), in which displacement currents are typically neglected. For a physically more complete description, the full set of Maxwell equations would be needed, including the time evolution equation of the electric field. Again, we split the MHD system into a first subsystem that contains the convective and the viscous terms that will both be discretized *explicitly*, whereas the second one is again the pure pressure subsystem that will be discretized *implicitly*, ie, we write

$$\frac{\partial\mathbf{Q}}{\partial t} + \nabla\cdot(\mathbf{F}^c - \mathbf{F}^v) + \nabla\cdot\mathbf{F}^p = 0, \tag{35}$$

with

$$\mathbf{F}^c = (\mathbf{f}^c, \mathbf{g}^c) = \begin{pmatrix} \rho\mathbf{v} \\ \rho\mathbf{v}\otimes\mathbf{v} + m\mathbf{I} - \frac{1}{4\pi}\mathbf{B}\otimes\mathbf{B} \\ \mathbf{v}^T(\rho k + 2m) - \frac{1}{4\pi}\mathbf{v}^T\mathbf{B}\otimes\mathbf{B} \\ \mathbf{B}\otimes\mathbf{v} - \mathbf{v}\otimes\mathbf{B} \end{pmatrix}, \quad \mathbf{F}^p = (\mathbf{f}^p, \mathbf{g}^p) = \begin{pmatrix} 0 \\ p\mathbf{I} \\ (\rho\mathbf{v})h \\ \mathbf{0} \end{pmatrix}. \tag{36}$$

4.2 | Semi-implicit discretization

The computational domain Ω is discretized by the control volumes of a primary grid denoted by $\Omega_{i,j} = [x_{i-\frac{1}{2}}, x_{i+\frac{1}{2}}] \times [y_{j-\frac{1}{2}}, y_{j+\frac{1}{2}}]$. To ease notation, in the following, we suppose an equidistant mesh spacing of size Δx and Δy in x and y direction and the corresponding number of cells is denoted by N_x and N_y, respectively. The edge-based staggered dual control volumes in x direction are denoted by $\Omega_{i+\frac{1}{2},i} = [x_i, x_{i+1}]\times[y_{j-\frac{1}{2}}, y_{j+\frac{1}{2}}]$, whereas the control volumes of the staggered dual grid in y direction are $\Omega_{i,j+\frac{1}{2}} = [x_{i-\frac{1}{2}}, x_{i+\frac{1}{2}}] \times [y_j, y_{j+1}]$, ie, overall the method uses a set of three overlapping grids, each of which entirely covers the domain Ω. The averaging operators from the main grid to the dual grids read

$$\mathbf{Q}^n_{i+\frac{1}{2},j} = \frac{1}{2}\left(\mathbf{Q}^n_{i,j} + \mathbf{Q}^n_{i+1,j}\right), \qquad \mathbf{Q}^n_{i,j+\frac{1}{2}} = \frac{1}{2}\left(\mathbf{Q}^n_{i,j} + \mathbf{Q}^n_{i,j+1}\right), \tag{37}$$

whereas the averaging from the two dual grids to the main grid is given by

$$\mathbf{Q}^n_{i,j} = \frac{1}{2}\left(\mathbf{Q}^n_{i-\frac{1}{2},j} + \mathbf{Q}^n_{i+\frac{1}{2},j}\right), \qquad \mathbf{Q}^n_{i,j} = \frac{1}{2}\left(\mathbf{Q}^n_{i,j-\frac{1}{2}} + \mathbf{Q}^n_{i,j+\frac{1}{2}}\right). \tag{38}$$

4.2.1 | Convective and viscous subsystem

The viscous and convective subsystem is discretized with an explicit finite volume scheme of the type

$$\mathbf{Q}^*_{i,j} = \mathbf{Q}^n_{i,j} - \frac{\Delta t}{\Delta x}\left(\mathbf{f}_{i+\frac{1}{2},j} - \mathbf{f}_{i-\frac{1}{2},j}\right) - \frac{\Delta t}{\Delta y}\left(\mathbf{g}_{i,j+\frac{1}{2}} - \mathbf{g}_{i,j-\frac{1}{2}}\right), \tag{39}$$

where the numerical fluxes at the element interfaces contain both the nonlinear convective as well as the viscous terms and therefore read

$$\begin{aligned}\mathbf{f}_{i+\frac{1}{2},j} = {} & \frac{1}{2}\left(\mathbf{f}^c\left(\mathbf{Q}^-_{i+\frac{1}{2},j}\right) + \mathbf{f}^c\left(\mathbf{Q}^+_{i+\frac{1}{2},j}\right)\right) - \frac{1}{2}s^x_{\max}\left(\mathbf{Q}^+_{i+\frac{1}{2},j} - \mathbf{Q}^-_{i+\frac{1}{2},j}\right) \\ & - \frac{1}{2}\left(\mathbf{f}^v\left(\mathbf{V}^n_{i+\frac{1}{2},j+\frac{1}{2}}, \nabla\mathbf{V}^n_{i+\frac{1}{2},j+\frac{1}{2}}\right) + \mathbf{f}^v\left(\mathbf{V}^n_{i+\frac{1}{2},j-\frac{1}{2}}, \nabla\mathbf{V}^n_{i+\frac{1}{2},j-\frac{1}{2}}\right)\right),\end{aligned} \tag{40}$$

with the boundary extrapolated values $\mathbf{Q}^{\pm}_{i+\frac{1}{2},j}$ and the maximum signal speed in x direction $s^x_{\max}$ computed as in the one-dimensional case. The expression for the numerical flux $\mathbf{g}_{i,j+\frac{1}{2}}$ is obviously very similar to the one for $\mathbf{f}_{i+\frac{1}{2},j}$; hence, it is not necessary to report it here. The second order MUSCL-Hancock scheme in two space dimensions is a straight-forward extension of the one-dimensional case shown previously and is well known, so we can omit the details. For the viscous flux, we define the *corner variables*

$$\mathbf{V}^n_{i+\frac{1}{2},j+\frac{1}{2}} = \frac{1}{4}\left(\mathbf{V}^n_{i,j} + \mathbf{V}^n_{i+1,j} + \mathbf{V}^n_{i,j+1} + \mathbf{V}^n_{i+1,j+1}\right) \tag{41}$$

and the *corner gradients* of the vector of primitive variables given by

$$\nabla\mathbf{V}^n_{i+\frac{1}{2},j+\frac{1}{2}} = \frac{1}{2}\left(\frac{\mathbf{V}^n_{i+1,j+1} - \mathbf{V}^n_{i,j+1}}{\Delta x} + \frac{\mathbf{V}^n_{i+1,j} - \mathbf{V}^n_{i,j}}{\Delta x}, \frac{\mathbf{V}^n_{i+1,j+1} - \mathbf{V}^n_{i+1,j}}{\Delta y} + \frac{\mathbf{V}^n_{i,j+1} - \mathbf{V}^n_{i,j}}{\Delta y}\right). \tag{42}$$

4.2.2 | Divergence-free evolution of the magnetic field

In multiple space dimensions, it is of fundamental importance to evolve the magnetic field in a consistent manner that respects the divergence-free condition $\nabla \cdot \mathbf{B} = 0$ exactly also on the discrete level. For this purpose, we follow the works of Balsara and Spicer[42,57] and introduce the magnetic field components on the staggered mesh as $(B_x)^n_{i+\frac{1}{2},j}$ and $(B_y)^n_{i,j+\frac{1}{2}}$. The normal magnetic field components can then be evolved in time by a discrete form of the induction Equation (33) as follows:

$$(B_x)^{n+1}_{i+\frac{1}{2},j} = (B_x)^n_{i+\frac{1}{2},j} - \frac{\Delta t}{\Delta y}\left(E^z_{i+\frac{1}{2},j+\frac{1}{2}} - E^z_{i+\frac{1}{2},j-\frac{1}{2}}\right), \tag{43}$$

$$(B_y)^{n+1}_{i,j+\frac{1}{2}} = (B_y)^n_{i,j+\frac{1}{2}} + \frac{\Delta t}{\Delta x}\left(E^z_{i+\frac{1}{2},j+\frac{1}{2}} - E^z_{i-\frac{1}{2},j+\frac{1}{2}}\right), \tag{44}$$

with the electric field component in z direction given by a multi-dimensional Riemann solver (see, eg, other works[58-63]) as

$$\begin{aligned}E^z_{i+\frac{1}{2},j+\frac{1}{2}} = {} & \frac{1}{2}v^n_{i+\frac{1}{2},j+\frac{1}{2}}\left((B_x)^n_{i+\frac{1}{2},j} + (B_x)^n_{i+\frac{1}{2},j+1}\right) - \frac{1}{2}s^y_{\max}\left((B_x)^n_{i+\frac{1}{2},j+1} - (B_x)^n_{i+\frac{1}{2},j}\right) \\ & - \frac{1}{2}u^n_{i+\frac{1}{2},j+\frac{1}{2}}\left((B_y)^n_{i,j+\frac{1}{2}} + (B_y)^n_{i+1,j+\frac{1}{2}}\right) + \frac{1}{2}s^x_{\max}\left((B_y)^n_{i+1,j+\frac{1}{2}} - (B_y)^n_{i,j+\frac{1}{2}}\right) \\ & + \eta\left(\partial_x(B_y)^n_{i+\frac{1}{2},j+\frac{1}{2}} - \partial_y(B_x)^n_{i+\frac{1}{2},j+\frac{1}{2}}\right).\end{aligned} \tag{45}$$

Note that, in (45), the last line accounts for the resistive term and is an approximation to the z component of the curl of $\mathbf{B}$ using the corner gradients computed in (42). The velocity vector in the corner has already been computed via (41). It is

easy to check that the scheme (43)-(44) is exactly divergence-free in the discrete sense

$$\frac{(B_x)^{n+1}_{i+\frac{1}{2},j} - (B_x)^{n+1}_{i-\frac{1}{2},j}}{\Delta x} + \frac{(B_y)^{n+1}_{i,j+\frac{1}{2}} - (B_y)^{n+1}_{i,j-\frac{1}{2}}}{\Delta y} = 0 \tag{46}$$

if the magnetic field was discretely divergence-free at the initial time $t = 0$. Note that, in 2D, it is sufficient to take $(B_z)^{n+1}_{i,j} = (B_z)^*_{i,j}$ from (39). After the update of the staggered magnetic fields B_x and B_y via (43)-(44), the cell-centered magnetic field vector $\mathbf{B}^{n+1}_{i,j}$ is obtained by averaging the staggered quantities back from the dual grid to the main grid. It has to be stressed that in the multidimensional case in general $\mathbf{B}^{n+1}_{i,j} \neq \mathbf{B}^*_{i,j}$, ie, the cell-centered quantity $\mathbf{B}^*_{i,j}$ obtained from (39) is only an auxiliary quantity that is *overwritten* by the averages onto the main grid of the consistently evolved magnetic field components $(B_x)^{n+1}_{i+\frac{1}{2},j}$ and $(B_y)^{n+1}_{i,j+\frac{1}{2}}$, which are the main quantities that represent the discrete magnetic field in our scheme. The cell-centered magnetic field is needed in order to compute the energy density of the magnetic field $m^{n+1}_{i,j}$ that is used later in the pressure subsystem.

4.2.3 | Pressure subsystem

In two space dimensions, the discrete momentum equations read

$$(\rho u)^{n+1}_{i+\frac{1}{2},j} = (\rho u)^*_{i+\frac{1}{2},j} - \frac{\Delta t}{\Delta x}\left(p^{n+1}_{i+1,j} - p^{n+1}_{i,j}\right), \quad (\rho v)^{n+1}_{i,j+\frac{1}{2}} = (\rho v)^*_{i,j+\frac{1}{2}} - \frac{\Delta t}{\Delta y}\left(p^{n+1}_{i,j+1} - p^{n+1}_{i,j}\right), \tag{47}$$

where pressure is taken *implicitly*, whereas all nonlinear convective and viscous terms have already been discretized *explicitly* via the operators $(\rho u)^*_{i+\frac{1}{2},j}$ and $(\rho v)^*_{i,j+\frac{1}{2}}$ given in (39). A preliminary form of the discrete total energy equation reads

$$\begin{aligned}\rho e\left(p^{n+1}_{i,j}, \rho^{n+1}_{i,j}\right) + m^{n+1}_{i,j} + (\tilde{\rho k})^{n+1}_{i,j} = (\rho E)^*_{i,j} &- \frac{\Delta t}{\Delta x}\left(\tilde{h}^{n+1}_{i+\frac{1}{2},j}(\rho u)^{n+1}_{i+\frac{1}{2},j} - \tilde{h}^{n+1}_{i-\frac{1}{2},j}(\rho u)^{n+1}_{i-\frac{1}{2},j}\right)\\ &- \frac{\Delta t}{\Delta y}\left(\tilde{h}^{n+1}_{i,j+\frac{1}{2}}(\rho v)^{n+1}_{i,j+\frac{1}{2}} - \tilde{h}^{n+1}_{i,j-\frac{1}{2}}(\rho v)^{n+1}_{i,j-\frac{1}{2}}\right).\end{aligned} \tag{48}$$

Here, we have used again the abbreviation $\rho e(p^{n+1}_{i,j}, \rho^{n+1}_{i,j}) = \rho^{n+1}_{i,j} e(p^{n+1}_{i,j}, \rho^{n+1}_{i,j})$. Inserting the discrete momentum Equations (47) into the discrete energy Equation (48) and making tilde symbols explicit via the simple Picard iteration, as in the one-dimensional case, leads to the following discrete wave equation for the unknown pressure:

$$\begin{aligned}\rho^{n+1}_{i,j} e\left(p^{n+1,r+1}_{i,j}, \rho^{n+1}_{i,j}\right) &- \frac{\Delta t^2}{\Delta x^2}\left(h^{n+1,r}_{i+\frac{1}{2},j}\left(p^{n+1,r+1}_{i+1,j} - p^{n+1,r+1}_{i,j}\right) - h^{n+1,r}_{i-\frac{1}{2},j}\left(p^{n+1,r+1}_{i,j} - p^{n+1,r+1}_{i-1,j}\right)\right)\\ &- \frac{\Delta t^2}{\Delta y^2}\left(h^{n+1,r}_{i,j+\frac{1}{2}}\left(p^{n+1,r+1}_{i,j+1} - p^{n+1,r+1}_{i,j}\right) - h^{n+1,r}_{i,j-\frac{1}{2}}\left(p^{n+1,r+1}_{i,j} - p^{n+1,r+1}_{i,j-1}\right)\right) = b^r_{i,j},\end{aligned} \tag{49}$$

with the known right-hand side

$$b^r_{i,j} = (\rho E)^*_{i,j} - m^{n+1}_{i,j} - (\rho k)^{n+1,r}_{i,j} - \frac{\Delta t}{\Delta x}\left(h^{n+1,r}_{i+\frac{1}{2},j}(\rho u)^*_{i+\frac{1}{2},j} - h^{n+1,r}_{i-\frac{1}{2},j}(\rho u)^*_{i-\frac{1}{2},j}\right) - \frac{\Delta t}{\Delta y}\left(h^{n+1,r}_{i,j+\frac{1}{2}}(\rho v)^*_{i,j+\frac{1}{2}} - h^{n+1,r}_{i,j-\frac{1}{2}}(\rho v)^*_{i,j-\frac{1}{2}}\right). \tag{50}$$

We stress that the density $\rho^{n+1}_{i,j} = \rho^*_{i,j}$ is already known from (39) and the energy of the magnetic field $m^{n+1}_{i,j}$ is already known after averaging the staggered normal magnetic field components that have been evolved via (43) and (44) onto the main grid. The system for the pressure (49) is again a mildly nonlinear system of the form (23) with a linear part that is symmetric and at least positive semidefinite. Hence, with the usual assumptions on the nonlinearity detailed in Casulli and Zanolli,[40] it can be again efficiently solved with the nested Newton method of Casulli and Zanolli.[39,40] Note that in the incompressible limit $M \to 0$, following the asymptotic analysis performed in other works,[100-104] the pressure tends to a constant and the contribution of the kinetic energy ρk can be neglected w.r.t. ρe. Therefore, in the incompressible limit, the system (49) tends to the usual pressure Poisson equation of incompressible flow solvers. In each Picard iteration, after the solution of the pressure system (49), the enthalpies at the interfaces can be recomputed and the momentum is updated by

$$(\rho u)^{n+1,r+1}_{i+\frac{1}{2},j} = (\rho u)^*_{i+\frac{1}{2},j} - \frac{\Delta t}{\Delta x}\left(p^{n+1,r+1}_{i+1,j} - p^{n+1,r+1}_{i,j}\right), \tag{51}$$

$$(\rho v)^{n+1,r+1}_{i,j+\frac{1}{2}} = (\rho v)^*_{i,j+\frac{1}{2}} - \frac{\Delta t}{\Delta y}\left(p^{n+1,r+1}_{i,j+1} - p^{n+1,r+1}_{i,j}\right), \tag{52}$$

from which $(\rho k)_{i,j}^{n+1,r+1}$ can be computed after averaging onto the main grid. At the end of the Picard iterations, the total energy is updated as

$$(\rho E)_{i,j}^{n+1} = (\rho E)_{i,j}^{*} - \frac{\Delta t}{\Delta x}\left(h_{i+\frac{1}{2},j}^{n+1} (\rho u)_{i+\frac{1}{2},j}^{n+1} - h_{i-\frac{1}{2},j}^{n+1} (\rho u)_{i-\frac{1}{2},j}^{n+1} \right) - \frac{\Delta t}{\Delta y}\left(h_{i,j+\frac{1}{2}}^{n+1} (\rho v)_{i,j+\frac{1}{2}}^{n+1} - h_{i,j-\frac{1}{2}}^{n+1} (\rho v)_{i,j-\frac{1}{2}}^{n+1} \right), \tag{53}$$

whereas the final momentum is averaged back onto the main grid. This completes the description of our new divergence-free semi-implicit algorithm for the VRMHD equations in the multidimensional case.

5 | NUMERICAL RESULTS IN 2D

In all the following numerical test problems, the ideal gas equation of state is used to make the results comparable with existing data in the literature. For applications with general EOS, see a previous work.[30] If not specified otherwise, the ratio of specific heats is chosen as $\gamma = 1.4$. The CPU timings reported in this section were obtained on a workstation using one single core of an Intel i7-2600 CPU with 3.4 GHz clock speed and 12 GB of RAM. In order to allow a better quantitative comparison with other schemes, we report the average CPU time that was needed to carry out one time step for one control volume, ie, dividing the total wall clock time needed by the simulation by the number of time steps and the number of control volumes. The inverse of this number corresponds to the number of zones which the scheme is able to update within one second of wall clock time on one CPU core. In the 2D simulations, the time step is computed according to

$$\Delta t = \mathrm{CFL} \frac{1}{\frac{\max|\lambda_x^c|}{\Delta x} + \frac{\max|\lambda_y^c|}{\Delta y} + 2\left(\frac{4}{3}\frac{\mu}{\rho} + \frac{\lambda}{c_v \rho} + \eta\right)\left(\frac{1}{\Delta x^2} + \frac{1}{\Delta y^2}\right)}, \tag{54}$$

with the Courant number $\mathrm{CFL} < 1$ and the "convective" eigenvalues λ_x^c and λ_y^c in x and y direction, respectively. In the above condition, also the contribution of the parabolic terms has been included, by simply adding all eigenvalues of the viscous and resistive operator, see, eg, the work by Dumbser,[105] for the eigenvalues of the viscous operator of the compressible Navier-Stokes equations. If not specified otherwise, we set $\mathrm{CFL} = 0.9$ in all test problems presented in this section. Furthermore, for all test cases, we have explicitly verified that up to machine precision the magnetic field is divergence-free and mass, momentum, and energy are conserved.

5.1 | Numerical convergence study

First of all, we carry out a numerical convergence study for the ideal inviscid MHD equations using a smooth MHD vortex problem similar to the one proposed for the first time by Balsara.[42] The computational domain is given by $\Omega = [0;10] \times [0;10]$ and periodic boundary conditions are applied in x and y direction. The ratio of specific heats is chosen as $\gamma = \frac{5}{3}$. The free parameters given in the aforementioned work[42] are chosen as $\epsilon = 1$ and $\tilde{\mu} = \sqrt{4\pi}$. The initial condition at time $t = 0$ in terms of primitive variables reads

$$\begin{pmatrix} \rho(\mathbf{x},0) \\ u(\mathbf{x},0) \\ v(\mathbf{x},0) \\ p(\mathbf{x},0) \\ B_x(\mathbf{x},0) \\ B_y(\mathbf{x},0) \end{pmatrix} = \begin{pmatrix} 1 \\ \frac{\epsilon}{2\pi} e^{\frac{1}{2}(1-r^2)}(5-y) \\ \frac{\epsilon}{2\pi} e^{\frac{1}{2}(1-r^2)}(x-5) \\ \frac{1}{8\pi}\left(\frac{\tilde{\mu}}{2\pi}\right)^2 (1-r^2) e^{(1-r^2)} - \frac{1}{2}\left(\frac{\epsilon}{2\pi}\right)^2 e^{(1-r^2)} \\ \frac{\tilde{\mu}}{2\pi} e^{\frac{1}{2}(1-r^2)}(5-y) \\ \frac{\tilde{\mu}}{2\pi} e^{\frac{1}{2}(1-r^2)}(x-5) \end{pmatrix}, \tag{55}$$

which is also the exact solution of the problem for all later times. The final simulation time is set to $t_{\mathrm{end}} = 1.0$. The L_2 error norms for a generic quantity q at time t^n are defined as

$$L_2(q, t^n) = \sqrt{\sum_{i,j} \Delta x \Delta y \left(q_{i,j}^n - q_e(x_i, y_j, t^n) \right)^2}, \tag{56}$$

TABLE 2 Numerical convergence results of the semi-implicit finite volume scheme for the ideal magnetohydrodynamics equations using a smooth magnetohydrodynamics vortex test problem. The L_2 error norms refer to the variables ρ (density), p (pressure), and B_x (magnetic field component in x direction) at the final time $t = 1.0$

$N_x = N_y$	$L_2(\rho,1)$	$\mathcal{O}(\rho)$	$L_2(p,1)$	$\mathcal{O}(p)$	$L_2(B_x,1)$	$\mathcal{O}(B_x)$
100	2.0037E-02		3.3675E-02		1.1598E-02	
200	6.1843E-03	1.7	1.0259E-02	1.7	3.4758E-03	1.7
300	2.9557E-03	1.8	4.7485E-03	1.9	1.6229E-03	1.9
400	1.7925E-03	1.7	2.7100E-03	1.9	9.4784E-04	1.9

where $q^n_{i,j}$ denotes the discrete solution and $q_e(x_i, y_j, t^n)$ the exact solution. In Table 2, we present numerical convergence results for the fluid density ρ, the pressure p, and the magnetic field component B_x obtained on a sequence of successively refined meshes. The number of grid cells used in x and y direction is denoted by N_x and N_y, respectively. In all cases, the time step size was kept constant and set to $\Delta t = 0.01$, and a second-order accurate MUSCL-Hancock scheme was used for the explicit nonlinear convective terms, ie, for the computation of the star quantities $\mathbf{Q}^*_{i,j}$. From our results, we can conclude that the scheme reaches second order of accuracy in space, as expected. Future work will concern an extension of our scheme to *arbitrary* order of accuracy in space and time using the family of staggered semi-implicit space-time DG finite element schemes recently introduced in other works.[106-108]

5.2 | Low Mach number magnetic field loop advection

Here, we solve the magnetic field loop advection problem proposed by Gardiner and Stone.[44] However, in order to make it more difficult and in order to show the performance of our new divergence-free semi-implicit finite volume scheme, we run the test case at *low Mach number*. The setup of the test problem is described in the following. The computational domain is $\Omega = [-1, 1]\times[-\frac{1}{2}, \frac{1}{2}]$ with four periodic boundary conditions everywhere. The initial density is set to $\rho = 1$, the initial velocity field is $\mathbf{v} = (2, 1, 0)$, the pressure is $p = 10^5$, and the initial magnetic field is prescribed by the magnetic

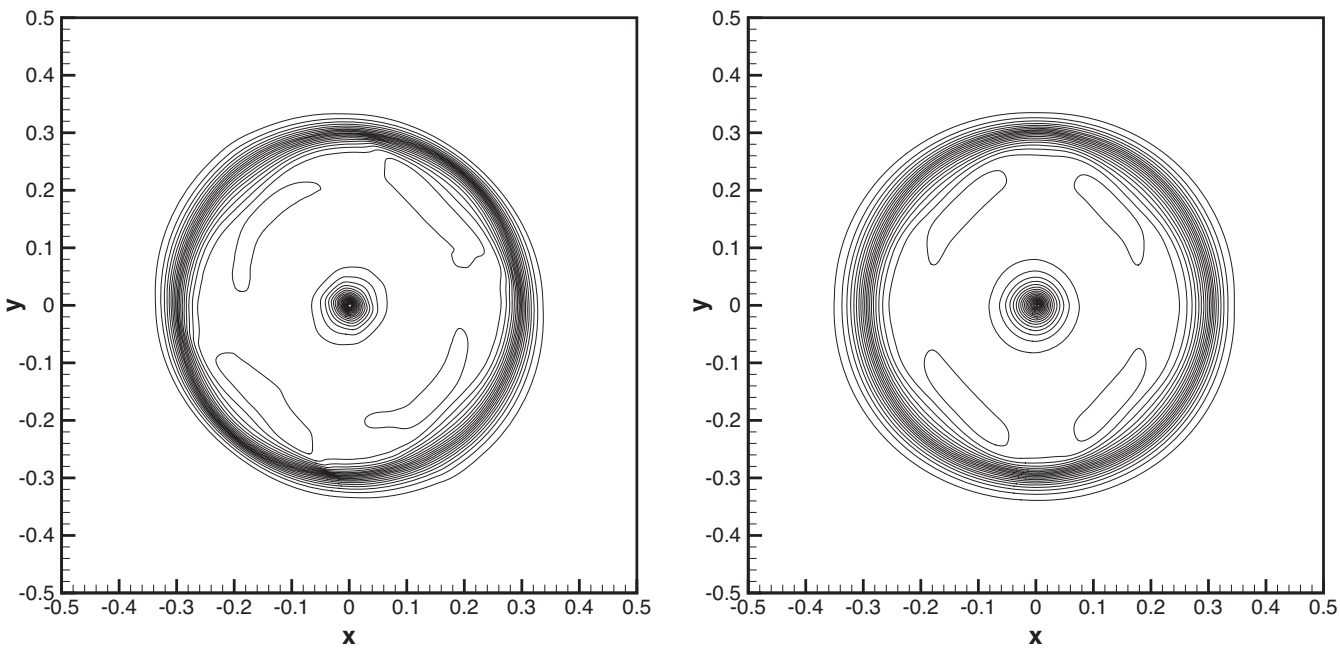

FIGURE 6 Numerical solution at time $t = 1.0$ obtained for the low Mach number magnetohydrodynamics field loop advection problem (see Section 5.2) with the divergence-free semi-implicit finite volume method (left) and with a divergence-free explicit second order Godunov-type scheme (right). Twenty equidistant contour lines of the magnetic field strength in the interval $[10^{-5}, 10^{-3}]$ are shown. For this test case, the density-based explicit scheme was more than a factor of 50 slower than the new pressure-based semi-implicit method

vector potential

$$A = \begin{cases} A_0(R - r) & \text{if} \quad r \leq R, \\ 0 & \text{if} \quad r > R, \end{cases} \tag{57}$$

with $A_0 = 10^{-3}$, $R = 0.3$ and $r^2 = x^2 + y^2$. The Mach number of the flow is about $M = 0.006$. We run the problem with the second-order version of our new semi-implicit FV scheme and with a divergence-free second-order explicit MUSCL-type TVD finite volume scheme[42,57] until $t = 1$ in order to complete one entire advection period. In both cases, the domain Ω is discretized with 500×250 control volumes and the CFL number is set to CFL $= 0.8$. The computational results for both cases (explicit vs semi-implicit) are depicted in Figure 6 and are comparable with those obtained in the literature, see, eg, other works,[44,50,58] although the explicit scheme appears to be slightly more dissipative, probably due to the extremely large number of time steps needed to reach the final time. The explicit method needed a total wall clock time of 78414 seconds, whereas our new semi-implicit FV scheme was able to complete the simulation in only 1356 seconds. This results in a speedup factor of **57** for the new semi-implicit scheme, which is a **clear advantage** for the new algorithm presented in this paper over existing schemes. For this simulation, the average computational cost of the SIFV scheme was 11.5μs per element and time step. The most expensive part here was the solution of the pressure system in the semi-implicit algorithm. For comparison, the average cost per element update for the explicit second order Godunov-type TVD scheme in this test was only 2μs per element and time step. However, since the explicit scheme needs *two orders of magnitude* more time steps compared to the semi-implicit scheme, the new SIFV method presented in this paper is still computationally much more efficient.

5.3 | Ideal MHD rotor problem

The well-known MHD rotor problem of Balsara and Spicer[57] has become a standard test bed for testing numerical methods for the ideal MHD equations. In this test a rotating high density fluid (the rotor) is embedded in a low density

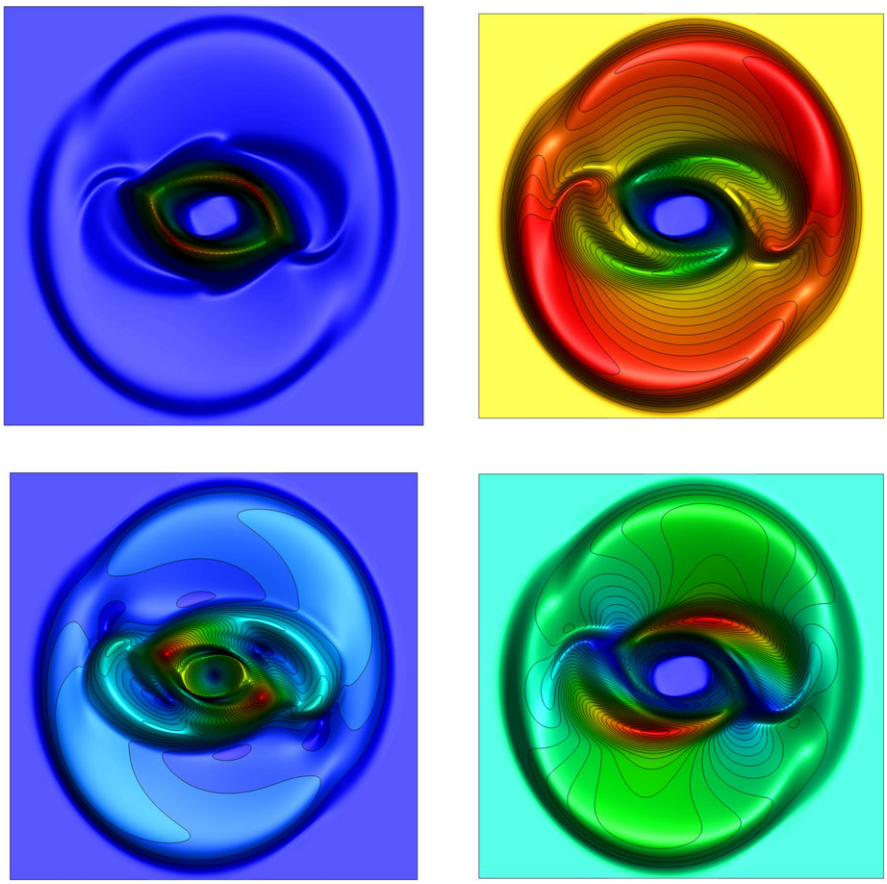

FIGURE 7 Numerical solution obtained with the divergence-free semi-implicit finite volume method for the magnetohydrodynamics rotor problem (see Section 5.3) at time $t = 0.25$. Contour lines of density (top left), pressure (top right), Mach number (bottom left) and magnetic pressure (bottom right) [Colour figure can be viewed at wileyonlinelibrary.com]

atmosphere at rest. Initially the pressure $p = 1$ and the magnetic field vector $\mathbf{B} = (2.5, 0, 0)^T$ are constant throughout the entire domain $\Omega = [-0.5, +0.5]^2$. The rotor produces torsional Alfvén waves which travel into the outer fluid at rest. The domain is discretized using a uniform Cartesian grid composed of 1000×1000 elements. For $0 \leq r \leq 0.1$, ie, inside the rotor, the initial density is $\rho = 10$, whereas it is set to $\rho = 1$ outside. The velocity field inside the rotor is set to $\mathbf{v} = \boldsymbol{\omega} \times \mathbf{x}$ with $\boldsymbol{\omega} = (0, 0, 10)$, whereas $\mathbf{v} = (0, 0, 0)$ in the outer fluid. The computational results obtained with the new divergence-free semi-implicit finite volume scheme at time $t = 0.25$ are shown in Figure 7 for the fluid density, the pressure, the Mach number as well as the magnetic pressure. The results agree qualitatively well with those obtained by Balsara and Spicer[57] and other results reported elsewhere in the literature, see, eg, other works.[46,47,50,58,99] The average computational cost of the SIFV scheme in this simulation was 3μs per element and time step.

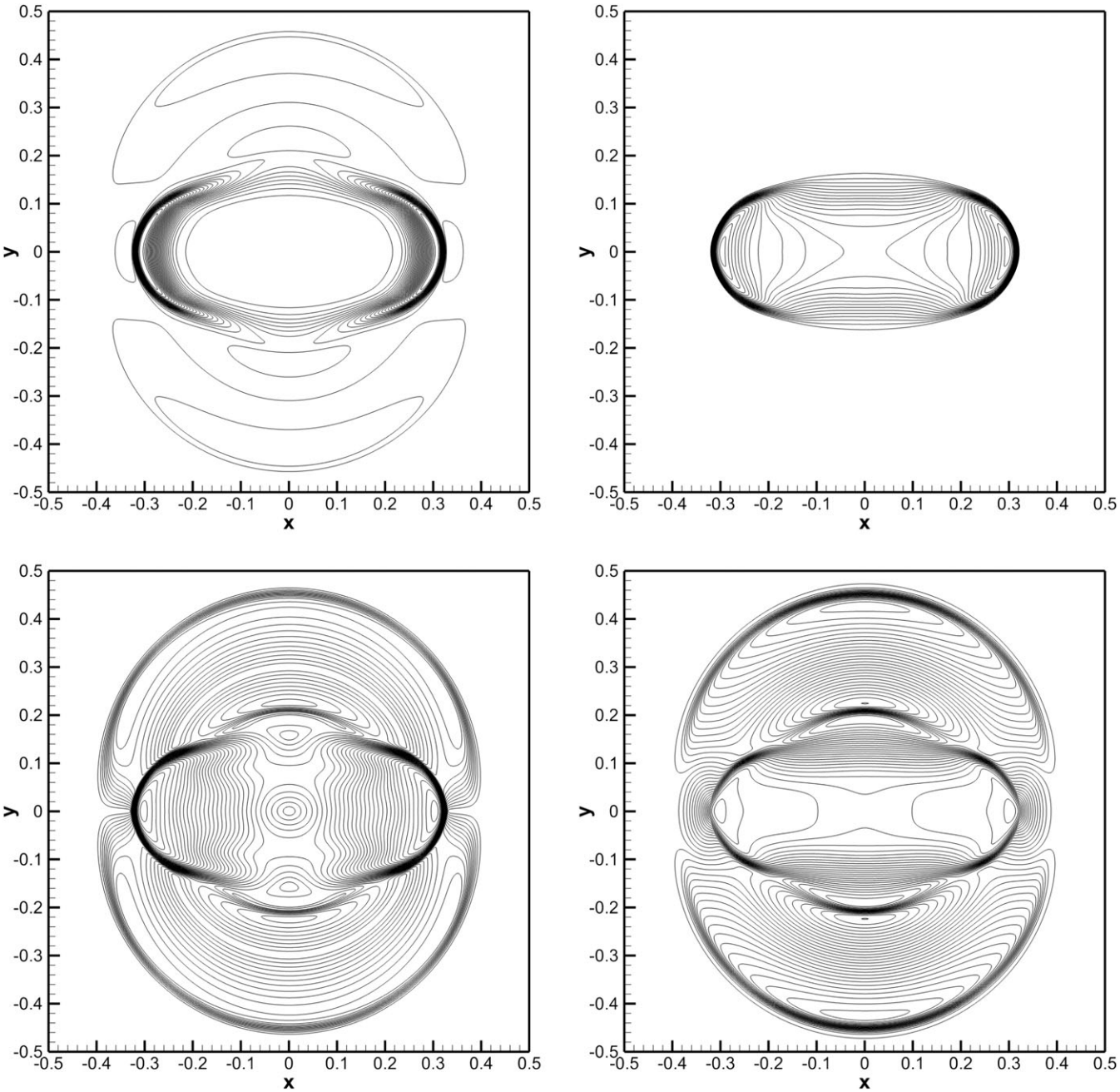

FIGURE 8 Numerical solution obtained with the divergence-free semi-implicit finite volume method for the magnetohydrodynamics blast wave problem (see Section 5.4) at time $t = 0.01$. Contour lines of density (top left), pressure (top right), velocity magnitude (bottom left) and magnetic pressure (bottom right)

5.4 | Ideal MHD blast wave problem

The MHD blast wave problem introduced in Balsara and Spicer[57] is a notoriously difficult test case. The initial data for density, velocity, and magnetic field are constant throughout the domain and are set to $\rho = 1$, $\mathbf{v} = (0,0,0)$, and $\mathbf{B} = (100,0,0)$. The pressure is initialized with $p = 1000$ in an inner circular region $r < 0.1$ and is set to $p = 0.1$ outside; hence, the pressure jumps over four orders of magnitude in this test problem. Furthermore, the fluid is highly magnetized due to the presence of a very strong magnetic field in the entire domain. The computational domain $\Omega = [-0.5, +0.5]^2$ is discretized with a uniform Cartesian grid using 1000×1000 pressure control volumes. The computational results obtained with our new divergence-free semi-implicit finite volume scheme at time $t = 0.01$ are presented in Figure 8 for the density, the pressure, the velocity magnitude, and the magnetic pressure. The results agree qualitatively with those obtained in the literature, see other works.[50,57,99] Moreover, for this test problem, the average computational cost of the SIFV scheme was 3μs per element and time step.

5.5 | Ideal MHD Orszag-Tang vortex

Here, we consider the very well-known Orszag-Tang vortex system for the ideal MHD equations, see other works[109-111] for a detailed discussion of the underlying flow physics. The computational setup is the one used in the work of Jiang and Wu[43] and a previous work[46] and is briefly summarized below. The computational domain under consideration is $\Omega = [0, 2\pi]^2$ with four periodic boundary conditions. The initial conditions are given by $\rho = \gamma^2$, $\mathbf{v} = (-\sin(y), \sin(x), 0)$, $p = \gamma$ and $\mathbf{B} = \sqrt{4\pi}(-\sin(y), \sin(2x), 0)$ with $\gamma = 5/3$. The computational domain is discretized with a uniform Cartesian mesh composed of 1000×1000 elements. The numerical results obtained with the SIFV scheme are shown in Figure 9 at times

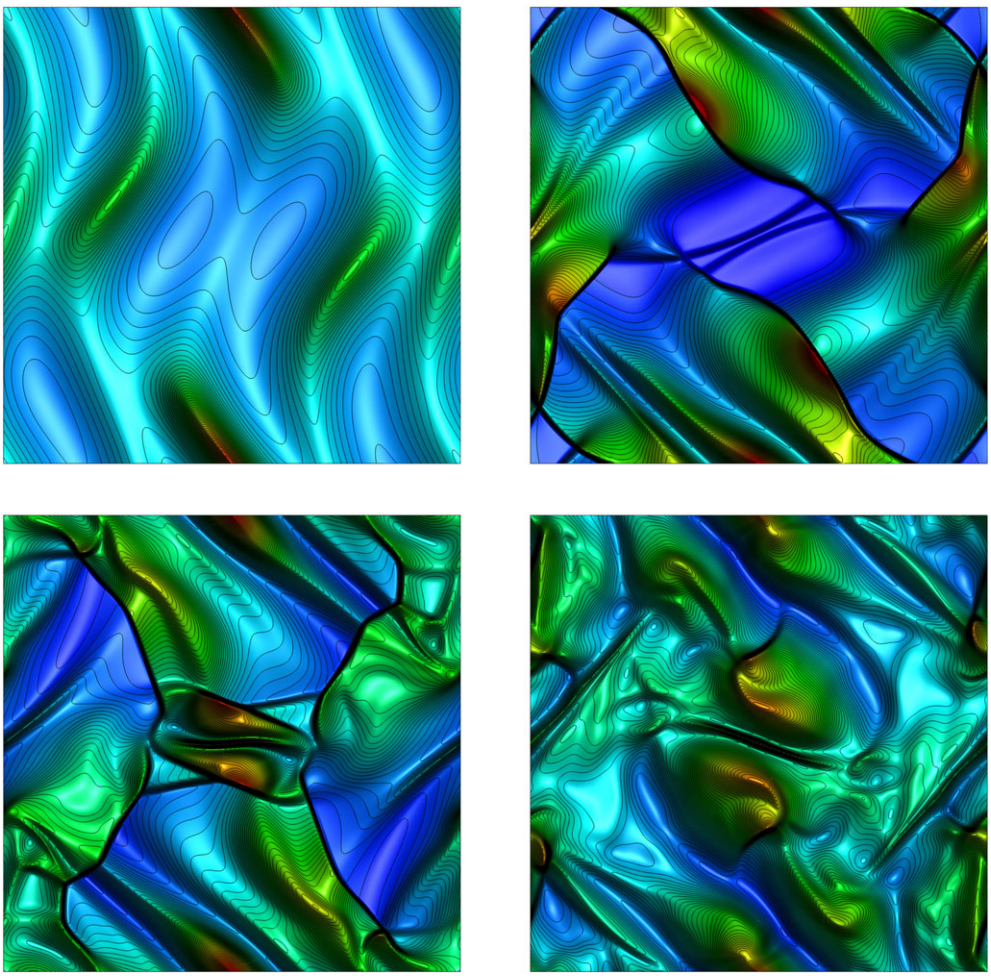

FIGURE 9 Numerical solution obtained with the divergence-free semi-implicit finite volume method for the inviscid Orszag-Tang vortex system (see Section 5.5) at time $t = 0.5$ (top left), $t = 2.0$ (top right), $t = 3.0$ (bottom left) and $t = 5.0$ (bottom right). 56 equidistant contour lines of the pressure are shown in the interval [0.5, 6] are shown [Colour figure can be viewed at wileyonlinelibrary.com]

$t = 0.5$, $t = 2.0$, $t = 3.0$, and $t = 5.0$ and agree qualitatively well with those presented elsewhere in the literature, see, eg, other works.[46,47,50,58,99] Moreover, for this test case, the average cost per element and time step was 3.0μs for the SIFV method. For comparison, the explicit second-order accurate divergence-free Godunov-type scheme needed 2.4μs per element and time step, ie, the average computational cost per element and time step of the semi-implicit scheme is only about 25% higher than for an analogous explicit method. Considering the fact that the semi-implicit scheme needs to solve $r_{\max}$ linear systems for the pressure in each time step (with $r_{\max} = 2$ being the number of chosen Picard iterations), this means that the overhead due to the implicit discretization of the pressure is only very small for this test problem. In our view, this is quite a remarkable result.

5.6 | VRMHD current sheet and shear layer at low Mach number

The current sheet and the simple shear layer (first problem of Stokes) are two very elementary test problems for the VRMHD equations, see, eg, Dumbser and Komissarov.[105,112] Since our new semi-implicit finite volume scheme is particularly well suited for low Mach number flows, we use the following initial conditions. In both cases, the density and the fluid pressure are set to $\rho = 1$ and $p = 10^5$, respectively. For the shear layer, the initial magnetic field is zero, and the velocity assumes the value $\mathbf{v}_L = (0, +1, 0)$ for $x \leq 0$ and $\mathbf{v}_R = (0, -1, 0)$ for $x > 0$. The exact solution is given by (see Schlichting and Gersten[113])

$$v(x,t) = -\mathrm{erf}\left(\frac{1}{2}\frac{x}{\sqrt{\mu t}}\right). \tag{58}$$

We emphasize that this setup would be very challenging for an explicit solver due to the large value of the pressure and the resulting low Mach number. For the current sheet, the velocity is initialized with zero, whereas the magnetic field is $\mathbf{B}_L = (0, +1, 0)$ for $x \leq 0$ and $\mathbf{B}_R = (0, -1, 0)$. The exact solution for B_y is the same as the one given in (58) for the shear layer. In both cases, the fluid parameters are $\eta = \mu = 0.1$, $Pr = 1$ and $c_v = 1$. All simulations have been carried out until $t = 0.1$ on the two-dimensional domain $\Omega = [-1, +1] \times [-0.1, +0.1]$ with periodic boundary conditions in y direction and using a uniform Cartesian mesh of 100×10 elements. For this test, we have deliberately chosen a 2D domain in order to check our particular divergence-free implementation of the resistivity term at the aid of a discrete double curl. In Figure 10, a scatter plot of the computational results obtained with the new divergence-free semi-implicit FV scheme is compared with the exact solution, where an excellent agreement can be observed for both cases. The scatter plot shows a clean one-dimensional behaviour, ie, no spurious two-dimensional modes are introduced by the double curl operator.

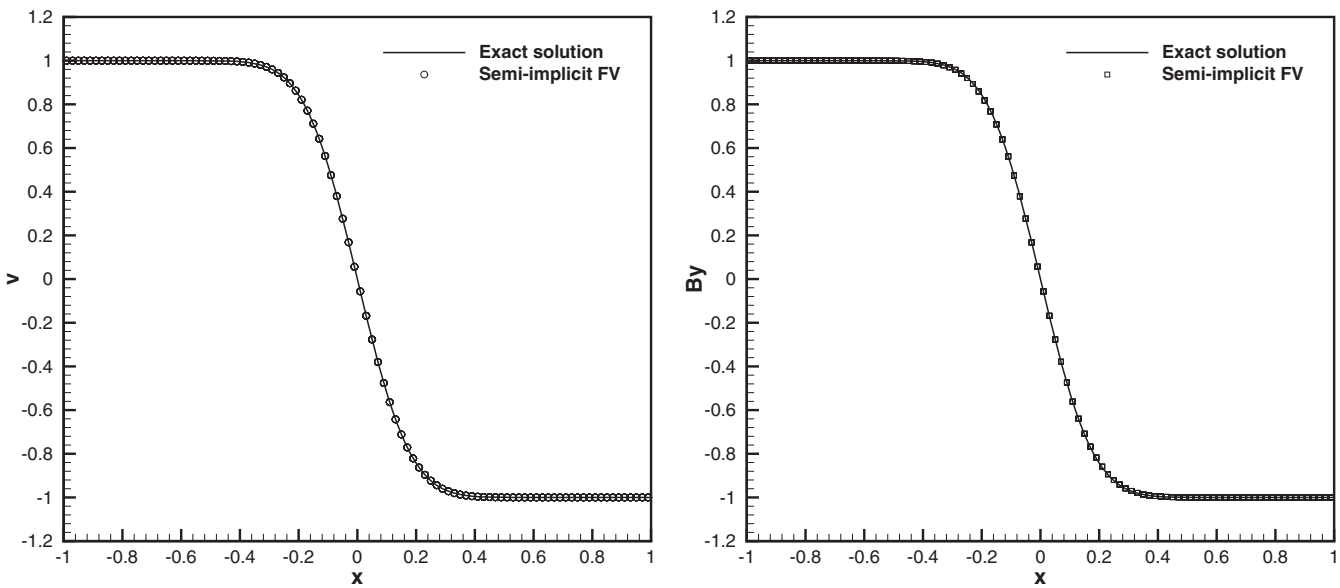

FIGURE 10 Exact and numerical solution for the low Mach number shear layer (left) and the current sheet (right) of Section 5.6 at time $t = 0.1$ solving the viscous and resistive magnetohydrodynamics equations with $\eta = \mu = 10^{-1}$. FV, finite volume

5.7 | VRMHD Orszag-Tang vortex

In this section, we solve the Orszag-Tang vortex system again but this time using the VRMHD equations. The fluid parameters are chosen as follows: $\gamma = \frac{5}{3}$, $\mu = \eta = 10^{-2}$, $c_v = 1$ and a Prandtl number of $Pr = 1$. The computational setup of this test case has been taken from the work of Warburton and Karniadakis[51] and a previous work[114] and is briefly summarized below. The computational domain is again $\Omega = [0, 2\pi]^2$ with four periodic boundary conditions, as in the inviscid case. The initial condition is given by $\rho = 1$, $\mathbf{v} = \sqrt{4\pi}(-\sin(y), \sin(x), 0)$, $\mathbf{B} = (-\sin(y), \sin(2x), 0)$ and $p = \frac{15}{4} + \frac{1}{4}\cos(4x) + \frac{4}{5}\cos(2x)\cos(y) - \cos(x)\cos(y) + \frac{1}{4}\cos(2y)$. Simulations are carried out on a uniform Cartesian grid of 500×500 elements until a final time of $t = 2$. The computational results obtained with the SIFV scheme are shown in Figure 11. They are also compared against a reference solution obtained in[114] at the aid of a very high order accurate

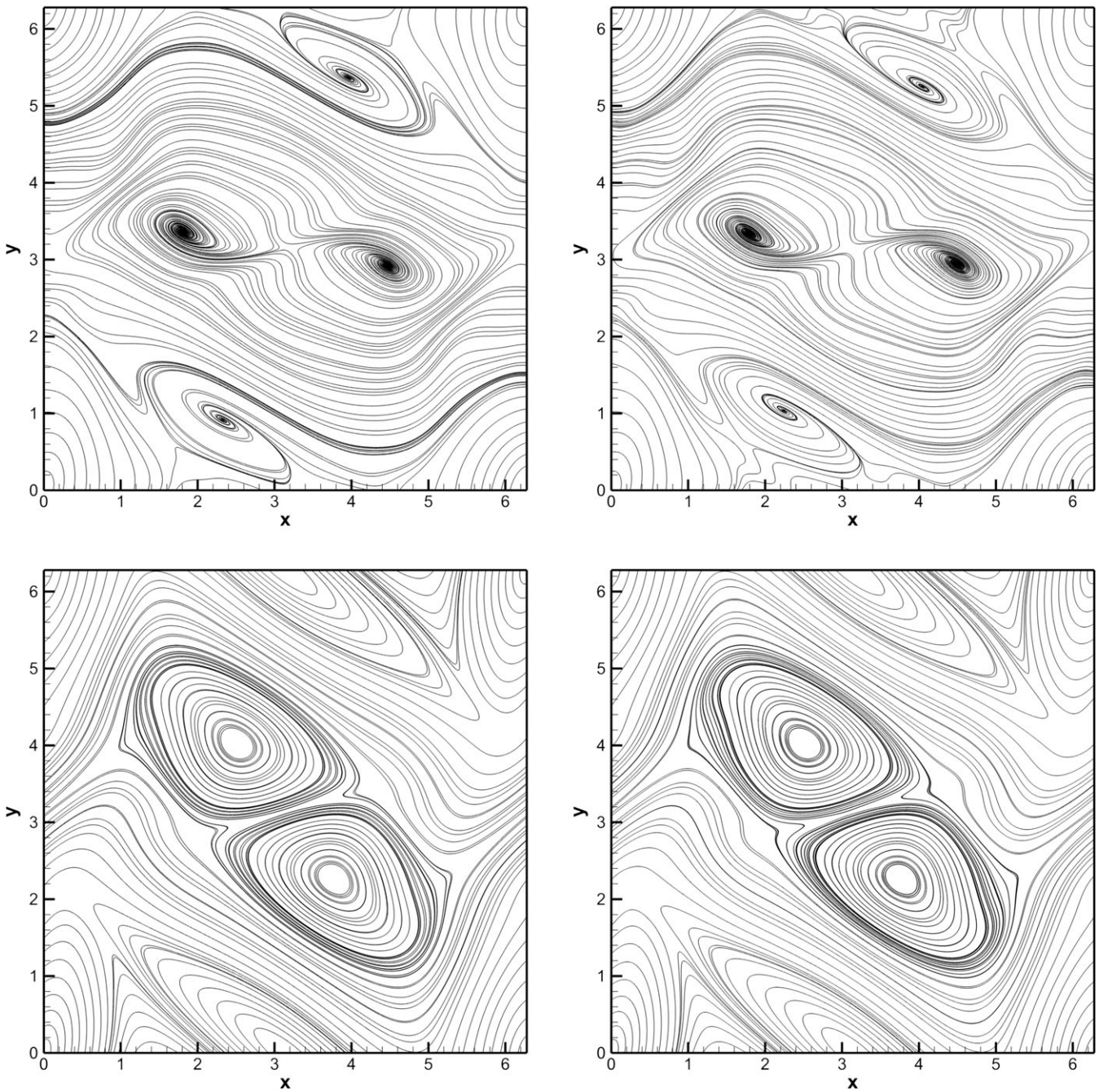

FIGURE 11 Reference solution (right) and numerical solution obtained with the new divergence-free semi-implicit finite volume method (left) for the viscous and resistive Orszag-Tang vortex of Section 5.7 ($\eta = \mu = 10^{-2}, Pr = 1$) at time $t = 2$. Velocity streamlines (top) and magnetic field lines (bottom)

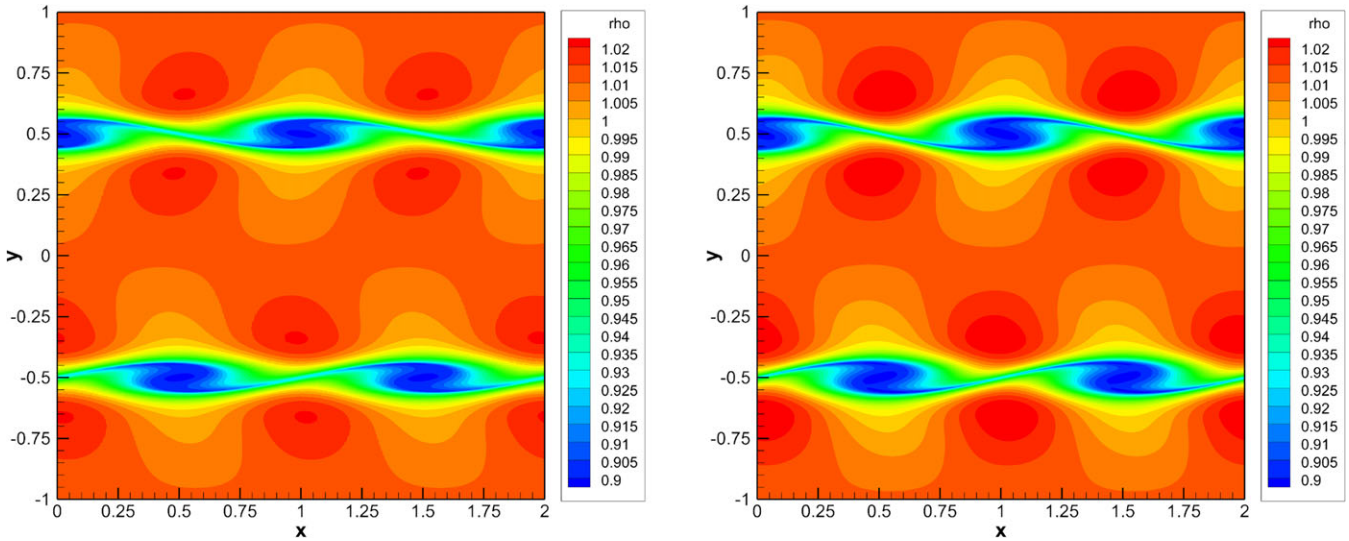

FIGURE 12 Reference solution (right) and numerical solution obtained with the new divergence-free semi-implicit finite volume method (left) for the viscous and resistive magnetohydrodynamics Kelvin-Helmholtz instability (see Section 5.8). The density contour levels are shown at the final time $t = 4.0$ [Colour figure can be viewed at wileyonlinelibrary.com]

$P_N P_M$ scheme. Overall, we can note a good agreement between the two solutions. The average computational cost for this simulation was also 3μs per element and time step, ie, the scheme is able to update more than $3.33 \cdot 10^5$ zones per second on one single CPU core.

5.8 | Kelvin-Helmholtz instability

In this test case, we consider the same setup as presented in the previous works[114,115] for the simulation of a Kelvin-Helmholtz instability developing in a viscous and resistive magnetized fluid. The initial condition is given by: $\rho = 1, p = \frac{3}{5}$,

$$\mathbf{v} = \left(-\frac{1}{2} U_0 \tanh\left(\frac{|y| - 0.5}{a} \right), \delta v \sin(2\pi x) \sin(\pi |y|), 0 \right),$$

$$\mathbf{B} = \begin{cases} (B_0, 0, 0), & \text{if} \quad \frac{1}{2} + a < |y| < 1, \\ (B_0 \sin(\chi), 0, B_0 \cos(\chi)), & \text{if} \quad \frac{1}{2} - a < |y| < \frac{1}{2} + a, \\ (0, 0, B_0), & \text{if} \quad 0 < |y| < \frac{1}{2} - a, \end{cases}$$

with $\chi = \frac{\pi}{2} \frac{y - 0.5 + a}{2a}$, $a = \frac{1}{25}$, $U_0 = 1$, $\delta v = 0.01$, and $B_0 = 0.07$. Furthermore $\gamma = \frac{5}{3}$, $\mu = \eta = 10^{-3}$, and we neglect the heat conduction by setting $\lambda = 0$. The computational domain is $\Omega = [0, 2] \times [-1, 1]$ using four periodic boundaries in all directions. For this test, we use 1000×1000 elements and run the simulation up to $t = 4s$. Figure 12 shows the comparison between the numerical solution obtained with the proposed SIFV method and the one obtained in the previous work[115] using a high-order explicit DG scheme for the solution of the VRMHD equations. A very good agreement can be observed also in this case that involves viscous and the resistive effects. The average computational cost for the new SIFV scheme was about 2.5μs per zone update.

6 | CONCLUSIONS

In this paper, we have presented a new divergence-free semi-implicit finite volume method for the simulation of the ideal, viscous, and resistive MHD equations with general EOS.

The split discretization of the nonlinear convective and viscous terms on the main grid combined with our very particular discretization of the pressure subsystem on a staggered grid allows us to reduce the final problem to the solution of a mildly nonlinear system for the fluid pressure, which can be efficiently solved by the (nested) Newton-type technique of Casulli et al.[37-40] The linear part of the mildly nonlinear system is given by a symmetric and positive semidefinite M-matrix,

which is a very remarkable property for a semi-implicit time discretization of the MHD equations. The nonlinearity in our mildly nonlinear system resides only on the diagonal and is contained in the equation of state that needs to provide the specific energy $e = e(p, \rho)$ as a function of the fluid pressure and the density. The EOS must must be a nonnegative non-decreasing function of p (for a given density), and its partial derivative w.r.t. p must be a function of bounded variation. For linear equations of state like the ideal gas EOS, the entire pressure system becomes linear and can therefore be solved in one single Newton iteration. The unknown kinetic energy at the new time level as well as the specific enthalpies are updated easily with a simple Picard process, following the suggestion of Casulli and Zanolli.[39] Once the pressure is known at the new time level, the momentum and total energy density can be readily obtained via a conservative update formula.

The magnetic field in our new SIFV scheme is also discretized on the staggered mesh, following the ideas of Balsara et al[58-63] on exactly divergence-free schemes for MHD and multidimensional Riemann solvers. In our method, the resistive terms in the induction equation are discretized using a discrete double curl formulation, which assures that the scheme remains exactly divergence free also in the nonideal (resistive) case.

The time step of our new method is only restricted by the fluid velocity and the speed of the Alfvén waves but not by the speed of sound. Therefore, our scheme is particularly well suited for **low Mach number flows**. For example, in the low Mach number magnetic field loop advection test presented in Section 5.2, our new semi-implicit method was more than **50 times faster** compared with a comparable explicit divergence-free second-order accurate Godunov-type finite volume scheme. Nevertheless, extensive numerical experiments have shown that our new pressure-based solver performs very well also for high Mach number flows with shock waves and other flow discontinuities. We have also compared the computational cost of the new SIFV scheme with the cost of a standard second-order Godunov-type scheme for MHD using the same code basis and the same computer to get a fair comparison. For example, for the Orszag-Tang vortex problem shown in Section 5.5 the average cost per element and time step of the explicit scheme was about 2.4μs, whereas it was about 3.0μs for the semi-implicit method, ie, despite the necessary solution of a linear system for the pressure in each of the two Picard iterations of the SIFV scheme, the semi-implicit method was only 25% more expensive than a fully explicit discretization. This means that we have a *very low overhead* because of the implicit discretization of the pressure subsystem, which in our opinion is also a remarkable result.

Future work will consist in an extension of the present approach to general unstructured meshes in multiple space dimensions and to higher order of accuracy at the aid of staggered semi-implicit DG finite element schemes, following the ideas outlined in other works.[106-108,116,117] In the near future we also plan an extension of this new family of efficient semi-implicit finite volume schemes to the unified Godunov-Peshkov-Romenski model of continuum mechanics[99,115,118] and to the Baer-Nunziato model of compressible multiphase flows,[119-121] where low Mach number problems are particularly important due to the simultaneous presence of two different phases.

ACKNOWLEDGEMENTS

The authors would like to thank S.A.E.G. Falle for providing the exact Riemann solver for the ideal MHD equations. The research presented in this paper was partially funded by the European Research Council (ERC) under the European Union's Seventh Framework Programme (FP7/2007-2013) within the research project *STiMulUs*, ERC Grant agreement no. 278267 and by the European Union's Horizon 2020 Research and Innovation Programme under the project *ExaHyPE*, grant no. 671698 (call FETHPC-1-2014). MD also acknowledges funding from the Italian Ministry of Education, University and Research (MIUR) in the frame of the Departments of Excellence Initiative 2018–2022 attributed to DICAM of the University of Trento, as well as financial support from the University of Trento in the frame of the *Strategic Initiative Modeling and Simulation*. The authors are also very grateful to the three anonymous referees and their constructive comments that were highly appreciated and which helped to improve the quality and clarity of the paper.

ORCID

M. Dumbser http://orcid.org/0000-0002-8201-8372
F. Fambri http://orcid.org/0000-0002-6070-8372

REFERENCES

1. Harlow FH, Welch JE. Numerical calculation of time-dependent viscous incompressible flow of fluid with a free surface. *Phys Fluids*. 1965;8:2182-2189.
2. Chorin AJ. A numerical method for solving incompressible viscous flow problems. *J Comput Phys*. 1967;2:12-26.

3. Chorin AJ. Numerical solution of the Navier-Stokes equations. *Math Comput*. 1968;23:341-354.
4. Patankar VS. *Numerical Heat Transfer and Fluid Flow*. New York, NY: Hemisphere Publishing Corporation; 1980.
5. Patankar VS, Spalding B. A calculation procedure for heat, mass and momentum transfer in three-dimensional parabolic flows. *Int J Heat Mass Transfer*. 1972;15:1787-1806.
6. Bell JB, Colella P, Glaz HM. A second-order projection method for the incompressible Navier-Stokes equations. *J Comput Phys*. 1989;85:257-283.
7. van Kan J. A second-order accurate pressure correction method for viscous incompressible flow. *SIAM J Sci Stat Comput*. 1986;7:870-891.
8. Hirt CW, Nichols BD. Volume of fluid (VOF) method for dynamics of free boundaries. *J Comput Phys*. 1981;39:201-225.
9. Casulli V. Semi-implicit finite difference methods for the two-dimensional shallow water equations. *J Comput Phys*. 1990;86:56-74.
10. Casulli V, Cheng RT. Semi-implicit finite difference methods for three-dimensional shallow water flow. *Int J Numer Methods Fluids*. 1992;15:629-648.
11. Casulli V. A semi-implicit finite difference method for non-hydrostatic free-surface flows. *Int J Numer Methods Fluids*. 1999;30:425-440.
12. Casulli V, Walters RA. An unstructured grid, three-dimensional model based on the shallow water equations. *Int J Numer Methods Fluids*. 2000;32:331-348.
13. Casulli V. A high-resolution wetting and drying algorithm for free-surface hydrodynamics. *Int J Numer Methods Fluids*. 2009;60:391-408.
14. Casulli V. A semi-implicit numerical method for the free–surface Navier–Stokes equations. *Int J Numer Methods Fluids*. 2014;74:605-622.
15. Casulli V, Greenspan D. Pressure method for the numerical solution of transient, compressible fluid flows. *Int J Numer Methods Fluids*. 1984;4(11):1001-1012.
16. Lax PD, Wendroff B. Systems of conservation laws. *Commun Pure Appl Math*. 1960;13:217-237.
17. Godunov SK. Finite difference methods for the computation of discontinuous solutions of the equations of fluid dynamics. *Mat Sb*. 1959;47:271-306.
18. Roe PL. Approximate Riemann solvers, parameter vectors, and difference schemes. *J Comput Phys*. 1981;43:357-372.
19. Osher S, Solomon F. Upwind difference schemes for hyperbolic conservation laws. *Math Comput*. 1982;38:339-374.
20. Harten A, Lax PD, van Leer B. On upstream differencing and Godunov-type schemes for hyperbolic conservation laws. *SIAM Review*. 1983;25(1):35-61.
21. Einfeldt B, Munz CD, Roe PL, Sjögreen B. On Godunov-type methods near low densities. *J Comput Phys*. 1991;92:273-295.
22. Munz CD. On Godunov–type schemes for Lagrangian gas dynamics. *SIAM J Numer Anal*. 1994;31:17-42.
23. Toro EF, Spruce M, Speares W. Restoration of the contact surface in the Harten-Lax-van Leer Riemann solver. *J Shock Waves*. 1994;4:25-34.
24. LeVeque RJ. *Finite Volume Methods for Hyperbolic Problems*. Cambridge, UK: Cambridge University Press; 2002.
25. Toro EF. *Riemann Solvers and Numerical Methods for Fluid Dynamics*. 3rd ed. Berlin, Germany: Springer; 2009.
26. Park JH, Munz CD. Multiple pressure variables methods for fluid flow at all mach numbers. *Int J Numer Methods Fluids*. 2005;49:905-931.
27. Cordier F, Degond P, Kumbaro A. An asymptotic-preserving all-speed scheme for the Euler and Navier-Stokes equations. *J Comput Phys*. 2012;231:5685-5704.
28. Kwatra N, Su J, Grétarsson JT, Fedkiw R. A method for avoiding the acoustic time step restriction in compressible flow. *J Comput Phys*. 2009;228:4146-4161.
29. Smolarkiewicz PK, Szmelter J. Iterated upwind schemes for gas dynamics. *J Comput Phys*. 2009;228:33-54.
30. Dumbser M, Casulli V. A conservative, weakly nonlinear semi-implicit finite volume method for the compressible Navier-Stokes equations with general equation of state. *Appl Math Comput*. 2016;272:479-497.
31. Boscarino S, Russo G, Scandurra L. All Mach number second order semi-implicit scheme for the Euler equations of gas dynamics. *J Sci Comput*. 2018. https://doi.org/10.1007/s10915-018-0731-9
32. Amari T, Luciani JF, Joly P. Preconditioned semi-implicit method for magnetohydrodynamics equations. *SIAM J Sci Comput*. 1999;21:970-986.
33. Lerbinger K, Luciani JF. A new semi-implicit method for MHD computations. *J Comput Phys*. 1991;97:444-459.
34. Harned DS, Kerner W. Semi-implicit method for three-dimensional resistive magnetohydrodynamic simulation of fusion plasmas. *Nuclear Sci Eng*. 1986;92:119-125.
35. Finan CH, Killeen J. Solution of the time-dependent, three-dimensional resistive magnetohydrodynamic equations. *Comput Phys Commun*. 1981;24:441-463.
36. Smolarkiewicz PK, Charbonneau P. EULAG, a computational model for multiscale flows: an MHD extension. *J Comput Phys*. 2013;236:608-623.
37. Brugnano L, Casulli V. Iterative solution of piecewise linear systems. *SIAM J Sci Comput*. 2007;30:463-472.
38. Brugnano L, Casulli V. Iterative solution of piecewise linear systems and applications to flows in porous media. *SIAM J Sci Comput*. 2009;31:1858-1873.
39. Casulli V, Zanolli P. A nested Newton-type algorithm for finite volume methods solving Richards' equation in mixed form. *SIAM J Sci Comput*. 2009;32:2255-2273.
40. Casulli V, Zanolli P. Iterative solutions of mildly nonlinear systems. *J Comput Appl Math*. 2012;236:3937-3947.
41. Falle SAEG, Komissarov SS, Joarder P. A multidimensional upwind scheme for magnetohydrodynamics. *J Comput Phys*. 1998;297:265-277.

42. Balsara DS. Second-order accurate schemes for magnetohydrodynamics with divergence-free reconstruction. *Astrophys J Supplement Series*. 2004;151:149-184.
43. Jiang GS, Wu CC. A high-order WENO finite difference scheme for the equations of ideal magnetohydrodynamics. *J Comput Phys*. 1999;150:561-594.
44. Gardiner TA, Stone JM. An unsplit Godunov method for ideal MHD via constrained transport. *J Comput Phys*. 2005;205:509-539.
45. Powell KG, Roe PL, Linde TJ, Gombosi TI, De Zeeuw DL. A solution-adaptive upwind scheme for ideal magnetohydrodynamics. *J Comput Phys*. 1999;154:284-309.
46. Dumbser M, Balsara DS, Toro EF, Munz CD. A unified framework for the construction of one-step finite-volume and discontinuous Galerkin schemes. *J Comput Phys*. 2008;227:8209-8253.
47. Dumbser M, Zanotti O, Hidalgo A, Balsara DS. ADER-WENO finite volume schemes with space-time adaptive mesh refinement. *J Comput Phys*. 2013;248:257-286.
48. Boscheri W, Dumbser M, Balsara DS. High order Lagrangian ADER-WENO schemes on unstructured meshes–application of several node solvers to hydrodynamics and magnetohydrodynamics. *Int J Numer Methods Fluids*. 2014;76:737-778.
49. Zanotti O, Fambri F, Dumbser M, Hidalgo A. Space-time adaptive ADER discontinuous Galerkin finite element schemes with a posteriori sub-cell finite volume limiting. *Comput Fluids*. 2015;118:204-224.
50. Balsara DS, Dumbser M. Divergence-free MHD on unstructured meshes using high order finite volume schemes based on multidimensional Riemann solvers. *J Comput Phys*. 2015;299:687-715.
51. Warburton T, Karniadakis G. A discontinuous Galerkin method for the viscous MHD equations. *J Comput Phys*. 1999;152:608-641.
52. Li F, Shu CW. Locally divergence-free discontinuous Galerkin methods for MHD equations. *J Sci Comput*. 2005;22:413-442.
53. Li F, Xu L. Arbitrary order exactly divergence-free central discontinuous Galerkin methods for ideal MHD equations. *J Comput Phys*. 2012;231:2655-2675.
54. Xu Z, Liu Y. New central and central discontinuous Galerkin schemes on overlapping cells of unstructured grids for solving ideal magnetohydrodynamic equations with globally divergence-free magnetic field. *J Comput Phys*. 2016;327:203-224.
55. Balsara DS, Käppeli R. Von Neumann stability analysis of globally divergence-free RKDG schemes for the induction equation using multidimensional Riemann solvers. *J Comput Phys*. 2017;336:104-127.
56. Liu Y, Shu CW, Zhang M. Entropy stable high order discontinuous Galerkin methods for ideal compressible MHD on structured meshes. *J Comput Phys*. 2018;354:163-178.
57. Balsara DS, Spicer D. A staggered mesh algorithm using high order Godunov fluxes to ensure solenoidal magnetic fields in magnetohydrodynamic simulations. *J Comput Phys*. 1999;149:270-292.
58. Balsara DS. Multidimensional HLLE Riemann solver: application to Euler and magnetohydrodynamic flows. *J Comput Phys*. 2010;229:1970-1993.
59. Balsara DS. A two-dimensional HLLC Riemann solver for conservation laws: application to Euler and magnetohydrodynamic flows. *J Comput Phys*. 2012;231:7476-7503.
60. Balsara DS. Three dimensional HLL Riemann solver for conservation laws on structured meshes: application to Euler and magnetohydrodynamic flows. *J Comput Phys*. 2015;295:1-23.
61. Balsara DS, Dumbser M, Abgrall R. Multidimensional HLLC Riemann solver for unstructured meshes–with application to Euler and MHD flows. *J Comput Phys*. 2014;261:172-208.
62. Balsara DS. Multidimensional Riemann problem with self-similar internal structure. Part I–application to hyperbolic conservation laws on structured meshes. *J Comput Phys*. 2014;277:163-200.
63. Balsara DS, Dumbser M. Multidimensional Riemann problem with self-similar internal structure. Part II–application to hyperbolic conservation laws on unstructured meshes. *J Comput Phys*. 2015;287:269-292.
64. Powell KG. *An Approximate Riemann Solver for Magnetohydrodynamics (That Works in More Than One Dimension)*. Technical Report. Hampton, VA: Institute for Computer Applications in Science and Engineering (ICASE); 1994.
65. Godunov SK. Symmetric form of the magnetohydrodynamic equation. *Numer Methods Mech Continuum Medium*. 1972;3(1):26-34.
66. Munz CD, Omnes P, Schneider R, Sonnendrücker E, Voss U. Divergence correction techniques for Maxwell solvers based on a hyperbolic model. *J Comput Phys*. 2000;161:484-511.
67. Dedner A, Kemm F, Kröner D, Munz CD, Schnitzer T, Wesenberg M. Hyperbolic divergence cleaning for the MHD equations. *J Comput Phys*. 2002;175:645-673.
68. Roe PL, Balsara DS. Notes on the eigensystem of magnetohydrodynamics. *SIAM J Appl Math*. 1996;56:57-67.
69. Casulli V, Cattani E. Stability, accuracy and efficiency of a semi-implicit method for three-dimensional shallow water flow. *Comput Math Appl*. 1994;27:99-112.
70. Van der Waals JD. *Over de Continuiteit van den Das-en Vloeistoftoestand*. Leiden, The Netherlands: Sijthoff; 1873.
71. Vidal J. *Thermodynamics: Applications in Chemical Engineering and the Petroleum Industry*. Paris, France: Editions Technip; 2001.
72. Peng DY, Robinson DP. A new two-constant equation of state. *Ind Eng Chem Fundam*. 1976;15:59-64.
73. Redlich O, Kwong JNS. On the thermodynamics of solutions. V. An equation of state. Fugacities of gaseous solutions. *Chem Rev*. 1949;44:233-244.
74. Wagner W, Cooper JR, Dittmann A, et al. The IAPWS industrial formulation 1997 for the thermodynamic properties of water and steam. *J Eng Gas Turbines Power*. 2000;122:150-182.
75. Wagner W, Pruss A. The IAPWS formulation 1995 for the thermodynamic properties of ordinary water substance for general and scientific use. *J Phys Chem Ref Data*. 2002;31:387-536.

76. Toro EF, Vázquez-Cendón ME. Flux splitting schemes for the Euler equations. *Comput Fluids*. 2012;70:1-12.
77. Steger JL, Warming RF. Flux vector splitting of the inviscid gas dynamic equations with applications to finite difference methods. *J Comput Phys*. 1981;40:263-293.
78. Zha GC, Bilgen E. Numerical solution of Euler equations by a new flux vector splitting scheme. *Int J Numer Methods Fluids*. 1993;17:115-144.
79. Liou MS, Steffen CJ. A new flux splitting scheme. *J Comput Phys*. 1993;107:23-39.
80. Balsara DS, Montecinos GI, Toro EF. Exploring various flux vector splittings for the magnetohydrodynamic system. *J Comput Phys*. 2016;311:1-21.
81. Casulli V, Stelling GS. Semi-implicit subgrid modelling of three-dimensional free-surface flows. *Int J Numer Methods Fluids*. 2011;67:441-449.
82. Casulli V, Dumbser M, Toro EF. Semi-implicit numerical modeling of axially symmetric flows in compliant arterial systems. *Int J Numer Methods Biomed Eng*. 2012;28:257-272.
83. Boscheri W, Dumbser M, Righetti M. A semi-implicit scheme for 3D free surface flows with high order velocity reconstruction on unstructured Voronoi meshes. *Int J Numer Methods Fluids*. 2013;72:607-631.
84. Fambri F, Dumbser M, Casulli V. An efficient semi-implicit method for three-dimensional non-hydrostatic flows in compliant arterial vessels. *Int J Numer Methods Biomed Eng*. 2014;30:1170-1198.
85. Dumbser M, Iben U, Ioriatti M. An efficient semi-implicit finite volume method for axially symmetric compressible flows in compliant tubes. *Appl Numer Math*. 2015;89:24-44.
86. Toro EF, Billet SJ. Centered TVD schemes for hyperbolic conservation laws. *IMA J Numer Anal*. 2000;20:44-79.
87. Toro EF, Hidalgo A, Dumbser M. FORCE schemes on unstructured meshes I: conservative hyperbolic systems. *J Comput Phys*. 2009;228:3368-3389.
88. Dumbser M, Hidalgo A, Castro M, Parés C, Toro EF. FORCE schemes on unstructured meshes II: non–conservative hyperbolic systems. *Comput Methods Appl Mech Eng*. 2010;199:625-647.
89. Brio M, Wu CC. An upwind differencing scheme for the equations of ideal magnetohydrodynamics. *J Comput Phys*. 1988;75:400-422.
90. Ryu D, Jones TW. Numerical magnetohydrodynamics in astrophysics: algorithm and tests for one-dimensional flow. *Astrophys J*. 1995;442:228-258.
91. Dai W, Woodward PR. Extension of the piecewise parabolic method to multidimensional ideal magnetohydrodynamics. *J Comput Phys*. 1994;115:485-514.
92. Dumbser M, Toro EF. On universal Osher-type schemes for general nonlinear hyperbolic conservation laws. *Commun Comput Phys*. 2011;10:635-671.
93. Falle SAEG, Komissarov SS. On the inadmissibility of non-evolutionary shocks. *J Plasma Phys*. 2001;65:29-58.
94. Falle SAEG. Rarefaction shocks, shock errors and low order of accuracy in ZEUS. *Astrophys J*. 2002;577:L123-L126.
95. Torrilhon M. Non-uniform convergence of finite volume schemes for Riemann problems of ideal magnetohydrodynamics. *J Comput Phys*. 2003;192:73-94.
96. Balsara DS. Total variation diminishing scheme for adiabatic and isothermal magnetohydrodynamics. *Astrophys J Suppl Ser*. 1998;116:133-153.
97. Torrilhon M, Balsara DS. High order WENO schemes: investigations on non-uniform convergence for MHD Riemann problems. *J Comput Phys*. 2004;201:586-600.
98. Glimm J. Solution in the large for nonlinear hyperbolic systems of equations. *Comm Pure Appl Math*. 1965;18:697-715.
99. Dumbser M, Peshkov I, Romenski E, Zanotti O. High order ADER schemes for a unified first order hyperbolic formulation of Newtonian continuum mechanics coupled with electro-dynamics. *J Comput Phys*. 2017;348:298-342.
100. Klainermann S, Majda A. Singular limits of quasilinear hyperbolic systems with large parameters and the incompressible limit of compressible fluid. *Commun Pure Appl Math*. 1981;34:481-524.
101. Klainermann S, Majda A. Compressible and incompressible fluids. *Commun Pure Appl Math*. 1982;35:629-651.
102. Klein R, Botta N, Schneider T, et al. Asymptotic adaptive methods for multi-scale problems in fluid mechanics. *J Eng Math*. 2001;39:261-343.
103. Munz CD, Roller S, Klein R, Geratz KJ. The extension of incompressible flow solvers to the weakly compressible regime. *Comput Fluids*. 2003;32:173-196.
104. Munz CD, Dumbser M, Roller S. Linearized acoustic perturbation equations for low Mach number flow with variable density and temperature. *J Comput Phys*. 2007;224:352-364.
105. Dumbser M. Arbitrary high order PNPM schemes on unstructured meshes for the compressible Navier-Stokes equations. *Comput Fluids*. 2010;39:60-76.
106. Tavelli M, Dumbser M. A staggered space-time discontinuous Galerkin method for the three-dimensional incompressible Navier-Stokes equations on unstructured tetrahedral meshes. *J Comput Phys*. 2016;319:294-323.
107. Tavelli M, Dumbser M. A pressure-based semi-implicit space-time discontinuous Galerkin method on staggered unstructured meshes for the solution of the compressible Navier-Stokes equations at all Mach numbers. *J Comput Phys*. 2017;341:341-376.
108. Fambri F, Dumbser M. Spectral semi-implicit and space-time discontinuous Galerkin methods for the incompressible Navier-Stokes equations on staggered Cartesian grids. *Appl Numer Math*. 2016;110:41-74.
109. Orszag SA, Tang CM. Small-scale structure of two-dimensional magnetohydrodynamic turbulence. *J Fluid Mech*. 1979;90:129.

110. Dahlburg RB, Picone JM. Evolution of the Orszag-Tang vortex system in a compressible medium. I. Initial average subsonic flow. *Phys Fluids B*. 1989;1:2153-2171.

111. Picone JM, Dahlburg RB. Evolution of the Orszag-Tang vortex system in a compressible medium. II. supersonic flow. *Phys Fluids B*. 1991;3:29-44.

112. Komissarov SS. Multidimensional numerical scheme for resistive relativistic magnetohydrodynamics. *Mon Not Roy Astr Soc*. 2007;382:995-1004.

113. Schlichting H, Gersten K. *Grenzschicht-Theorie*. Berlin, Germany: Springer; 2005.

114. Dumbser M, Balsara DS. High-order unstructured one-step PNPM schemes for the viscous and resistive MHD equations. *Comput Modeling Eng Sci*. 2009;54:301-333.

115. Dumbser M, Peshkov I, Romenski E, Zanotti O. High order ADER schemes for a unified first order hyperbolic formulation of continuum mechanics: viscous heat-conducting fluids and elastic solids. *J Comput Phys*. 2016;314:824-862.

116. Dumbser M, Casulli V. A staggered semi-implicit spectral discontinuous Galerkin scheme for the shallow water equations. *Appl Math Comput*. 2013;219(15):8057-8077.

117. Fambri F, Dumbser M. Semi-implicit discontinuous Galerkin methods for the incompressible Navier-Stokes equations on adaptive staggered Cartesian grids. *Comput Methods Appl Mech Eng*. 2017;324:170-203.

118. Peshkov I, Romenski E. A hyperbolic model for viscous Newtonian flows. *Continuum Mech Thermodyn*. 2016;28:85-104.

119. Baer MR, Nunziato JW. A two-phase mixture theory for the deflagration-to-detonation transition (DDT) in reactive granular materials. *J Multiphase Flow*. 1986;12:861-889.

120. Saurel R, Abgrall R. A multiphase Godunov method for compressible multifluid and multiphase flows. *J Comput Phys*. 1999;150:425-467.

121. Saurel R, Abgrall R. A simple method for compressible multifluid flows. *SIAM J Sci Comput*. 1999;21:1115-1145.

How to cite this article: Dumbser M, Balsara DS, Tavelli M, Fambri F. A divergence-free semi-implicit finite volume scheme for ideal, viscous, and resistive magnetohydrodynamics. *Int J Numer Meth Fluids*. 2019;89:16–42. https://doi.org/10.1002/fld.4681